Control Engineering Practice 139 (2023) 105620

Contents lists available at ScienceDirect

Control Engineering Practice

journal homepage: www.elsevier.com/locate/conengprac

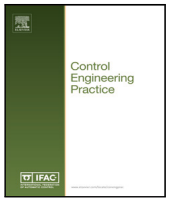

A sensor fault detection, isolation, and estimation method for intelligent vehicles

Tenglong Huang, Huihui Pan *, Weichao Sun

Research Institute of Intelligent Control and Systems, Harbin Institute of Technology, Harbin, 150001, China

ARTICLE INFO

Keywords:
Intelligent vehicles
Sensor fault
Interval bounds
Fault detection
Isolation
Estimation

ABSTRACT

Accurate and reliable sensor information is crucial for intelligent vehicles to ensure safety and reliability. It is significant to devise effective solutions to diagnose possible sensor faults. In this paper, a sensor fault detection, isolation, and estimation approach is developed for intelligent vehicle-integrated motion systems. The Luenberger observer is designed and embedded into the fault diagnosis framework to real-time estimate the system states. Interval observers are constructed for vehicle subsystems to estimate the interval bounds of the corresponding observation errors. The estimation errors enter into the corresponding intervals generated by the adaptive laws when the sensor fault is free. In the event of a sensor fault, it can be detected efficiently and the faulty sensor can be isolated. Moreover, occurred sensor fault can be estimated by modifying the interval observer structure. The simulation results in the standard J-Turn test scenario are provided to evaluate and verify the effectiveness of the proposed method.

1. Introduction

Intelligent vehicles (Feng et al., 2023; Huang, Pan, Sun, & Gao, 2022; Pan, Chang, & Sun, 2023; Pan, Hong, Sun, & Jia, 2023; Spielberg, Brown, Kapania, Kegelman, & Gerdes, 2019; Wang, Zhang, Ahn, & Xu, 2021) equipped with numerous sensors can acquire accurate real-time vehicle state information and achieve superior perception capabilities, which is the cornerstone for ensuring that vehicles can cope with complex traffic environments and accomplish advanced decision, planning, and control tasks. More sensors contribute to realizing advanced and sophisticated functionalities, however, the probability and risk of sensor fault occurrences also increase correspondingly. The sensor fault (Kommuri, Defoort, Karimi, & Veluvolu, 2016) means that the current information feedback is inaccurate or even incorrect and is a severe fault. In general, compared with actuator faults (Pan, Zhang, Sun, & Yu, 2022; Wang & Deng, 2019; Wang, Ma, Pan, & Sun, 2023; Wang, Pan, & Zhang, 2023), sensor faults cause much greater system performance degradation. When sensor faults occur, timely detection of the fault location and fault estimation contribute to reducing the adverse effects caused by the sensor fault by employing hardware or software redundancy. Therefore, when a sensor fault (Samy, Postlethwaite, & Gu, 2011) occurs, it is essential to perform fault detection, isolation, and estimation for enhancing the system reliability which is also the focus of this paper.

The existing sensor fault (Holzmann, Halfmann, Germann, Würtenberger, & Isermann, 1997; Karimi, Chadli, Shi, & Zhang, 2014; Li, Karimi, Zhang, Zhao, & Li, 2017) diagnosis methods mainly include signal-based, knowledge-based, and model-based diagnosis approaches (Samy et al., 2011). Rich results about signal analysis-based fault diagnosis approaches existed in the literature, however, this method is sometimes not sensitive to potential faults. Knowledge-based methods for detecting sensor faults rely on associating fault features with relevant knowledge. Nevertheless, valid and enough knowledge is difficult to collect. Neural networks (Pan, Zhang, & Sun, 2022; Wang, Gao, Zhao, & Ahn, 2020) can be employed to detect faults online, however, the implementation of the network structure is complicated. Additionally, ensuring adequate and effective training of the designed network poses a significant challenge. Model-based fault diagnosis approaches rely on the system model characteristics and require model information. Vehicles are an important part of modern industry and research into modeling has yielded a wealth of results. Therefore, employing existing research on vehicle modeling to design a model-based approach (Shen, Yue, Goh, & Wang, 2018) for avoiding the above-mentioned problems is possible while achieving effective fault diagnosis.

Model-based methods, including weighted-least squares (Havyarimana et al., 2023), linear matrix inequality (Karimi, Duffie, & Dashkovskiy, 2010; Karimi & Gao, 2008; Karimi, Zapateiro, & Luo, 2010; Pertew, Marquez, & Zhao, 2007), Kalman filtering (Borguet & Léonard, 2009) and interval observer (Blesa, Rotondo, Puig, & Nejjari, 2014; Puig et al., 2006; Wang, 2020; Zhang & Yang, 2017), etc, have been successfully applied to fault diagnosis, which can detect, isolate, or estimate fault effectively. Weighted-least squares can cope with linear models, nonetheless, are difficult to deal with model uncertainties arising from nonlinear properties. Meanwhile, the performance

* Corresponding author.
E-mail address: huihuipan@hit.edu.cn (H. Pan).

https://doi.org/10.1016/j.conengprac.2023.105620
Received 28 December 2022; Received in revised form 12 June 2023; Accepted 1 July 2023
Available online 24 July 2023

degradation of linear Kalman filtering also occurred caused by the model uncertainties. Constrained Kalman filtering can cope with uncertain parameters, however, the computational burden is expensive. It is noteworthy that interval observers (Efimov, Raissi, & Zolghadri, 2013; Raïssi, Videau, & Zolghadri, 2010) offer distinct advantages in addressing disturbances and uncertainties, thereby garnering great attention. When the sensor is fault-free, the corresponding state is located at a reasonable interval. The upper and lower bounds of the state interval can be used to detect, isolate, and estimate the fault. Nevertheless, traditional interval observers require prior information about perturbations and uncertainties to determine its interval range. This paper, therefore, aims to design an interval observer which can adaptively estimate interval range without the prior information of perturbation and uncertainties.

Another challenge is the high complexity of the vehicle model when multiple subsystems are considered. Most of the existing fault diagnosis methods for vehicles are developed for one of the dynamics subsystems. For example, for the vehicle vertical subsystem with model uncertainty, Yan, Sun, He, and Yao (2018) proposes a fault diagnosis method that can adaptively detect and isolate occurred faults. An event-triggered zonotope-based fault diagnosis strategy is designed in Wang, Fei, Yan, and Xu (2020), which is applied to the vehicle lateral dynamic subsystem. The probabilistic fault diagnosis strategy presented in Oh, Park, Lee, and Yi (2018) can detect the sensor fault in the vehicle longitudinal dynamic. Strong coupling and interactions exist between different subsystems of intelligent vehicles, especially the lateral and longitudinal dynamics, which improves the model complexity and makes it difficult to design fault diagnosis methods. Therefore, sensor fault diagnosis for vehicle lateral-longitudinal dynamics is more challenging. Accordingly, this paper seeks an effective fault diagnosis method for the coupled vehicle lateral-longitudinal dynamics, which attempts to address the disturbance, and dynamics uncertainties and achieve effective fault diagnosis.

As discussed above, it is unrealistic to determine the interval bounds of conventional interval observers when lateral and longitudinal vehicle dynamics are taken into account. Meanwhile, the threshold setting for classical fixed-threshold fault detection methods poses difficulties. Therefore, developing an adaptive sensor fault detection, isolation, and estimation approach is necessary. This paper proposes an adaptive model-based framework for detecting, isolating, and estimating sensor faults in vehicle lateral-longitudinal coupled dynamical systems, taking into account disturbances and uncertainties. Specifically,

- A state estimation method based on the Luenberger observer is constructed for lateral-longitudinal coupled dynamical systems, which allows for efficient state estimation. Meanwhile, the observer errors with reasonable observer gains are proved to be bounded.
- The interval observers without dependence on the prior knowledge of perturbation and uncertainties are constructed. In the absence of sensor faults, the constructed interval observers allow for the estimation of the state to enter the estimated interval boundary even in the presence of perturbations and uncertainties. Additionally, the proposed interval observers can be adapted to estimate corresponding faults interval bounds effectively, thereby enabling sensor fault detection and isolation.
- Further, a modification to the interval observer structure is proposed and utilized to estimate the occurred sensor fault corresponding to the faulty sensor. This modified interval observer allows for effective adaptive estimation of the upper and lower boundaries of the sensor fault interval.

The rest of this paper is organized as follows. The vehicle model, containing the lateral and longitudinal vehicle dynamics, is briefly introduced in Section 2, while the problem is stated and related lemmas are provided. The main results of the paper are summarized in Section 3, including the presented state observer, and the interval observers structures designed for different subsystems. Meanwhile, the corresponding theorems and proofs are detailed in this section. The analysis and proof of the modified interval observer for the faulty sensor are also provided in this section. The presented sensor fault detection, isolation, and estimation framework, for the vehicle with lateral and longitudinal dynamics, in Section 2 is then validated with simulation results in Section 4. Finally, the paper is concluded in Section 5.

2. Vehicle modeling and problem statement

The kinematic relations and the lateral-longitudinal coupled dynamics model of intelligent vehicles are formulated in this section. Additionally, the sensor faults considered in this paper for intelligent vehicles are described detailedly. Meanwhile, the necessary preliminaries are given in this section.

2.1. Vehicle model formulation

The kinematic relation of intelligent vehicle can be expressed as

$$\dot{\xi} = \mathcal{T}(\varphi)\vartheta \tag{1}$$

where $\xi := [\xi_x, \xi_y, \varphi]^{\mathrm{T}}$, $\vartheta := \left[\vartheta_x, \vartheta_y, \varpi\right]^{\mathrm{T}}$, and the coordinate transformation matrix is defined as $\mathcal{T}(\varphi) := [\cos\varphi \ -\sin\varphi \ 0; \ \sin\varphi \ \cos\varphi \ 0; \ 0 \ 0 \ 1]$. (ξ_x, ξ_y) represent vehicle position information in Cartesian coordinates. ϑ_x and ϑ_y denote the vehicle longitudinal and lateral velocity in the body-fixed coordinate system, respectively. φ and ϖ are the vehicle yaw angle and yaw rate.

As in Fig. 1, a detailed illustration of the intelligent vehicle containing lateral, longitudinal, and yaw dynamics is plotted. The detailed definitions and key parameters of the vehicle are provided in Table 1, which are the same as the parameters settings in Zhang, Sun, and Du (2019). The vehicle dynamics model, as derived in Huang, Wang, Pan, and Sun (2022), Sun, Zhang, and Liu (2018), Zhang et al. (2019), can be written as

$$\begin{cases} \dot{\vartheta}_x &= \vartheta_y\varpi - \frac{C_l}{M}\vartheta_x^2 + \frac{1}{MR_e}\left(\upsilon_1+\upsilon_2\right) - f_{n1} + d_1 \\ \dot{\vartheta}_y &= -\frac{(C_a+C_b)\vartheta_y}{M\vartheta_x} + \left(\frac{C_bd_b-C_ad_a}{M\vartheta_x} - \vartheta_x\right)\varpi + \frac{C_a}{M}\upsilon_3 \\ & \quad + f_{n2} + d_2 \\ \dot{\varpi} &= \frac{(C_bd_b-C_ad_a)\vartheta_y-(C_ad_a^2+C_bd_b^2)\varpi}{I_z\vartheta_x} - \frac{d_c}{I_zR_e}\left(\upsilon_1-\upsilon_2\right) \\ & \quad + \frac{C_ad_a}{I_z}\upsilon_3 + f_{n3} + d_3 \end{cases} \tag{2}$$

where $d := \left[d_1, d_2, d_3\right]^{\mathrm{T}}$ is the external disturbance. $f_n := \left[f_{n1}, f_{n2}, f_{n3}\right]^{\mathrm{T}}$ (Huang, Wang, et al., 2022) denotes the unmodeled nonlinear terms. The vector $\upsilon := \left[\upsilon_1, \upsilon_2, \upsilon_3\right]^{\mathrm{T}}$ is defined as

$$\begin{cases} \upsilon_1 = T_{al}\cos\theta_a + T_{bl} \\ \upsilon_2 = T_{ar}\cos\theta_a + T_{br} \\ \upsilon_3 = \theta_a \end{cases} \tag{3}$$

where T_{ij} denotes the wheel torque, $i = a/b$ represent the front or rear wheel, and $j = r/l$ are the right of left wheel. Define $u := \left[u_1, u_2, u_3\right]^{\mathrm{T}}$, $u_1 = \frac{1}{MR_e}\left(\upsilon_1+\upsilon_2\right)$, $u_2 = \frac{C_a}{M}\upsilon_3$, and $u_3 = \frac{C_ad_a}{I_z}\upsilon_3 - \frac{d_c}{I_zR_e}\left(\upsilon_1-\upsilon_2\right)$, the kinematic and dynamic model can be expressed as

$$\dot{\xi} = \mathcal{T}(\varphi)\vartheta \tag{4}$$

$$\dot{\vartheta} = \mathcal{L}(\vartheta)\vartheta + f_n + u + d \tag{5}$$

where

$$\mathcal{L}(\vartheta) = \begin{bmatrix} \frac{-\vartheta_xC_a}{M} & \varpi & 0 \\ 0 & -\frac{C_a+C_b}{M\vartheta_x} & \frac{C_bd_b-C_ad_a}{M\vartheta_x} - \vartheta_x \\ 0 & \frac{C_bd_b-C_ad_a}{\vartheta_xI_z} & \frac{-C_bd_b^2-C_ad_a^2}{\vartheta_xI_z} \end{bmatrix}$$

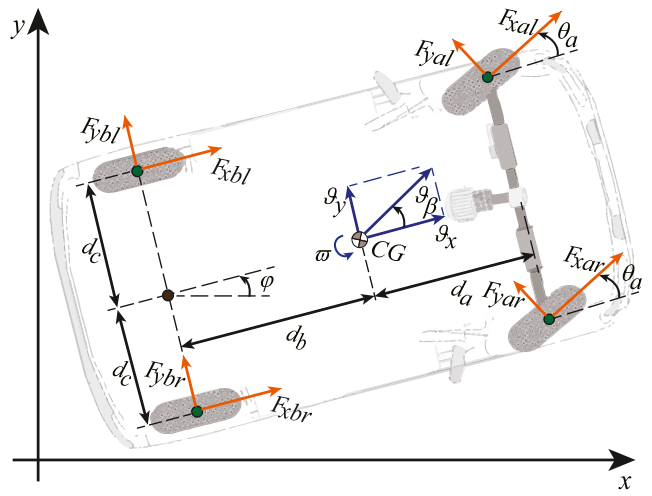

Fig. 1. Illustration of intelligent vehicles containing lateral, longitudinal, and yaw dynamics.

Table 1
Parameters descriptions.

Symbol	Value	Definition	Unit
I_z	1343.1	Moment of Inertial around z-axis	kg m^2
C_a	22010	Front Wheel Cornering Stiffness	N/rad
$\mathcal{R}_e$	0.31	Effective Radius of Wheel	m
d_b	1.56	Distance from Rear Axle to CG	m
C_1	0.05	Aerodynamic Drag Factor	N s^2/m^2
d_a	1.04	Distance from Front Axle to CG	m
M	1110	Vehicle Total Mass	kg
d_c	0.74	Half Width of the Wheel Track	m
C_b	22010	Rear Wheel Cornering Stiffness	N/rad

Define $\mathcal{V} := \left[\mathcal{V}_x, \mathcal{V}_y, \mathcal{V}_w\right]^{\mathrm{T}}$ as the vehicle velocity vector in the global coordinate system, we get

$$\dot{\xi} = \mathcal{V} \tag{6}$$

$$\dot{\mathcal{V}} = \mathcal{Q}(\xi, \mathcal{V}, t) + \mathcal{T}(\varphi)u + \mathcal{W}(\xi, \mathcal{V}, t) \tag{7}$$

where $\mathcal{Q} := \mathcal{P}(\varpi)\mathcal{V} + \mathcal{T}(\varphi)\mathcal{L}\left(\xi, \mathcal{T}^{\mathrm{T}}\mathcal{V}\right)\mathcal{T}^{T}\mathcal{V}$, $\mathcal{W} := \mathcal{T}(\varphi)\left(f_n + d\right)$, and $\mathcal{P}(\varpi) := [0\ -\varpi\ 0; \varpi\ 0\ 0;\ 0\ 0\ 0]$. The corresponding reference signals can be expressed as $\xi_r := [\xi_{xr}, \xi_{yr}, \varphi_r]^{\mathrm{T}}$ and $\mathcal{V}_r := \left[\mathcal{V}_{xr}, \mathcal{V}_{yr}, \mathcal{V}_{wr}\right]^{\mathrm{T}}$.

Define the error signals $\mathcal{E}_1 := \xi - \xi_r$ and $\mathcal{E}_2 := \mathcal{V} - \mathcal{V}_r$, the vehicle integrated motion control error model without sensor faults can be expressed as

$$\dot{\mathcal{E}}_1 = \mathcal{E}_2 \tag{8}$$

$$\dot{\mathcal{E}}_2 = \mathcal{I} + \mathcal{Z} \tag{9}$$

$$\mathcal{O}_1 = \mathcal{J}_1\mathcal{E}_1,\ \mathcal{O}_2 = \mathcal{J}_2\mathcal{E}_2 \tag{10}$$

where $\mathcal{I} := \mathcal{T}(\varphi)u - \ddot{\xi}_r$, and $\mathcal{Z} := \mathcal{Q}(\xi, \mathcal{V}, t) + \mathcal{W}(\xi, \mathcal{V}, t)$. $\mathcal{J}_1 = [1\ 0\ 0; 0\ 1\ 0; 0\ 0\ 1]$ and $\mathcal{J}_2 = \mathcal{J}_1$ denote output matrixes of the position and attitude subsystem and velocity subsystem, respectively. The corresponding measurement outputs are defined as $\mathcal{O}_1$ and $\mathcal{O}_2$, respectively.

2.2. Problem statement

This paper focuses on designing a sensor fault detection, isolation, and estimation scheme for intelligent vehicles. The mathematical model of intelligent vehicles is briefly introduced above in (1)–(10). Specifically, for the intelligent vehicles described in (6) and (7), a method is proposed to implement sensor faults detection. Meanwhile, the sensor fault isolation is achieved and the faulty sensor can be identified. Then, the upper and lower bounds of the sensor fault are estimated.

2.3. Preliminaries

Lemma 1. *Given a matrix $\mathcal{D} \in \mathbb{R}^{p\times q}$, the corresponding matrices $\mathcal{D}^+$ and $\mathcal{D}^-$ can be calculated as $\mathcal{D}^+ = \max\{\mathcal{D}, 0\}$ and $\mathcal{D}^- = \mathcal{D}^+ - \mathcal{D}$. Meanwhile, in this paper, for vectors or matrices $\varkappa_1$ and $\varkappa_2$, $\varkappa_1 < \varkappa_2$ means that every element in $\varkappa_1$ is smaller than the corresponding element in $\varkappa_2$. For a constant matrix $\mathcal{D}$ and q -dimensional vectors $\varkappa$, $\overline{\varkappa}$, and $\underline{\varkappa}$ which satisfy $\underline{\varkappa} \le \varkappa \le \overline{\varkappa}$, then we have (Chebotarev, Efimov, Raïssi, & Zolghadri, 2015)*

$$\mathcal{D}^+\underline{\varkappa} - \mathcal{D}^-\overline{\varkappa} \le \mathcal{D}\varkappa \tag{11}$$

$$\mathcal{D}^+\overline{\varkappa} - \mathcal{D}^-\underline{\varkappa} \ge \mathcal{D}\varkappa \tag{12}$$

Lemma 2. *If the off-principal diagonal elements of $\mathcal{D}_1$ are non-negative and $\mathcal{D}_1$ is a Hurwitz matrix, $\mathcal{D}_1$ is a Metzler matrix. Given the system which can be expressed in the following form (Raïssi et al., 2010)*

$$\dot{\varsigma}(t) = \mathcal{D}_M\varsigma(t) + \varsigma_f(t), \quad \varsigma(0) = \varsigma_0 \tag{13}$$

where $\mathcal{D}_M$ is a Metzler matrix, then $\varsigma > 0$, $\forall\ t > 0$ holds when $\varsigma_f(t) > 0$ and the initial vector $\varsigma_0 > 0$.

3. Main results

In this section, the Luenberger observer is designed firstly to estimate the system states. Then interval observers are constructed for $\mathcal{O}_1$ subsystem and $\mathcal{O}_2$ subsystem to estimate the state observation errors. The upper and lower bounds of the estimation errors in the absence of sensor faults can be estimated adaptively by the constructed interval observers. The occurrence of a sensor fault can result in a deviation between the measured output and the corresponding estimation, causing it to exceed the estimation interval. Further, modified interval observers are introduced to adaptively estimate the sensor fault. The proposed sensor faults detection, isolation, and estimation framework is detailed in this section.

3.1. Observer design

To estimate the error signals in (8)–(10), the following Luenberger observer is introduced

$$\dot{\hat{\mathcal{E}}}_1 = \hat{\mathcal{E}}_2 + C_1(\mathcal{O}_1 - \hat{\mathcal{O}}_1) \tag{14}$$

$$\dot{\hat{\mathcal{E}}}_2 = \mathcal{I} + C_2(\mathcal{O}_2 - \hat{\mathcal{O}}_2) \tag{15}$$

where $\hat{\mathcal{E}}_1$ and $\hat{\mathcal{E}}_2$ denote the estimates of $\mathcal{E}_1$ and $\mathcal{E}_2$ respectively. C_1 :=diag(C_{11}, C_{12}, C_{13}) and C_2 :=diag(C_{21}, C_{22}, C_{23}) are positive constant diagonal matrices that denote the observer gains. $\hat{\mathcal{O}}_1 := \mathcal{J}_1\hat{\mathcal{E}}_1$ and $\hat{\mathcal{O}}_2 := \mathcal{J}_2\hat{\mathcal{E}}_2$ are the estimations of the output vectors $\mathcal{O}_1$ and $\mathcal{O}_2$. Define the observer estimation error as follows

$$\Xi_1 = \mathcal{E}_1 - \hat{\mathcal{E}}_1, \Xi_2 = \mathcal{E}_2 - \hat{\mathcal{E}}_2 \tag{16}$$

Correspondingly, the output estimation error can be expressed as

$$\Xi_{\mathcal{O}1} = \mathcal{O}_1 - \hat{\mathcal{O}}_1, \Xi_{\mathcal{O}2} = \mathcal{O}_2 - \hat{\mathcal{O}}_2 \tag{17}$$

According to (14)–(17), the estimated error dynamics can be derived as follows

$$\dot{\Xi}_1 = -C_1\mathcal{J}_1\Xi_1 + \Xi_2,\ \Xi_{\mathcal{O}1} = \mathcal{J}_1\Xi_1 \tag{18}$$

$$\dot{\Xi}_2 = -C_2\mathcal{J}_2\Xi_2 + \mathcal{Z},\ \Xi_{\mathcal{O}2} = \mathcal{J}_2\Xi_2 \tag{19}$$

where the $\mathcal{Z}$ is assumed to be bounded, namely $\mathcal{Z} < \overline{\mathcal{Z}}$. The bound information $\overline{\mathcal{Z}}$ is unknown.

Define $Y_1 := -C_1\mathcal{J}_1, Y_2 := -C_2\mathcal{J}_2, \Psi_1 := I_3, \mathcal{Z}_1 := \Xi_2, \Psi_2 := I_3, \mathcal{Z}_2 := \mathcal{Z}$ with I_3 denotes 3×3 identity matrix. The derivatives of the estimation errors (18) and (19) can be rewritten as follows

$$\dot{\Xi}_1 = Y_1\Xi_1 + \Psi_1\mathcal{Z}_1, \Xi_{\mathcal{O}1} = \mathcal{J}_1\Xi_1 \tag{20}$$

$$\dot{\Xi}_2 = Y_2\Xi_2 + \Psi_2\mathcal{Z}_2, \Xi_{\mathcal{O}2} = \mathcal{J}_2\Xi_2 \tag{21}$$

Theorem 1. *By employing the observer constructed in (14) and (15) with observer gains $C_1 > 0$, $C_2 > 0$, the observation errors $\Xi_i, i = 1,2$ and output estimation errors $\Xi_{\mathcal{O}i}$ are bounded and converge exponentially to a neighborhood of 0. The convergence performance of the observation errors Ξ_i and output estimation errors $\Xi_{\mathcal{O}i}$ depend on the observer gains C_1 and C_2.*

Proof. From (20) and (21), it is obvious that $Y_i, i = 1,2$ is a diagonal constant matrix and subject to $Y_i < 0$. For simplicity, for each observation error $\Xi_{2j}, j = 1,2,3$ in ((21)), we can obtain $\dot{\Xi}_{2j} = Y_{2j}\Xi_{2j} + \Psi_{2j}\mathcal{Z}_{2j}, j = 1,2,3$. Ξ_{ij}, $\Xi_{\mathcal{O}ij}$, $\overline{\mathcal{Z}}_j$ and Ψ_{ij} denote the elements at the j th row of Ξ_i, $\Xi_{\mathcal{O}i}$, $\overline{\mathcal{Z}}$ and Ψ_i, respectively. $\mathcal{J}_{ij}$ and Y_{ij} represent the element on the jth row and jth column of $\mathcal{J}_i$ and Y_i, which are subject to $Y_{ij} < 0$. According to $\mathcal{Z} < \overline{\mathcal{Z}}$, we can get $\dot{\Xi}_{2j} < Y_{2j}\Xi_{2j} + \Psi_{2j}\overline{\mathcal{Z}}_j$. Consequently, for (21), it follows that $\Xi_{2j}(t) < \Xi_{2j}(0)e^{Y_{2j}t} + \frac{\Psi_{2j}\overline{\mathcal{Z}}_j}{Y_{2j}}\left(1 - e^{Y_{2j}t}\right)$. Thus, it can be inferred that the observation error Ξ_{2j} and the corresponding output estimation error are bounded. Namely, there exists a bound $\overline{\Xi}_2$ such that $\Xi_2 < \overline{\Xi}_2$. Similarly, for (20), we have $\Xi_{1j}(t) < \Xi_{1j}(0)e^{Y_{1j}t} + \frac{\Psi_{1j}\overline{\Xi}_{2j}}{Y_{1j}}\left(1 - e^{Y_{2j}t}\right), j = 1,2,3$. Obviously, the convergence performance of Ξ_i and $\Xi_{\mathcal{O}i}$ depend on the observer parameters C_1 and C_2. Above, it is obvious that the observation errors Ξ_i and output estimation errors $\Xi_{\mathcal{O}i}$ are bounded and the exponential convergence property is proved. ■

Remark 1. An integrated motion controller is designed for vehicle motion systems based on nonlinear sliding mode theory. The sliding surface ϱ is chosen as $\varrho := \mathcal{K}_1\mathcal{E}_1 + \mathcal{E}_2$. The detailed controller form can be described as

$$u = \mathcal{T}(\varphi)^T\left\{-\mathcal{K}_1\mathcal{E}_2 - \mathcal{Q}(\xi, \mathcal{V}, t) + \dot{\mathcal{V}}_r - \mathcal{K}_d\text{sign}(\varrho)\right\} \tag{22}$$

where $\mathcal{K}_1 := \text{diag}(\mathcal{K}_{11}, \mathcal{K}_{12}, \mathcal{K}_{13}) > 0$ is the positive diagonal controller gain matrix. And the positive diagonal matrix $\mathcal{K}_d := \text{diag}(\mathcal{K}_{d1}, \mathcal{K}_{d2}, \mathcal{K}_{d3}) > 0$ is the robust parameter. The stability of the fault-free vehicle can be proved by selecting the Lyapunov function candidate $\mathcal{V}c = \frac{1}{2}\varrho^T\varrho$ and employing the stability theory. It can be demonstrated that the system is stable with controller (22) when $\mathcal{K}_d$ is sufficiently large.

Subsequently, interval observers are designed and introduced for subsystems Ξ_1 and Ξ_2 in (20) and (21) to estimate the observation errors of the Luenberger observer in (14) and (15). The real error signal can be obtained according to the measurement signals when the sensors for position, attitude, and velocity are healthy, namely, the sensor faults are free. In this case, the observation errors Ξ_1 and Ξ_2 lie within a reasonable interval by selecting the suitable Luenberger observer gains C_1 and C_2. The interval observers constructed for subsystems (20) and (21) allow for adaptive estimation of the upper and lower boundaries of the corresponding intervals.

First, the interval observer for the Ξ_1 subsystem in (20) is designed as follows

$$\dot{\overline{\Xi}}_1 = Y_1\overline{\Xi}_1 + \Psi_1^+\overline{\mathcal{Z}}_1 - \Psi_1^-\underline{\mathcal{Z}}_1 \tag{23}$$

$$\dot{\underline{\Xi}}_1 = Y_1\underline{\Xi}_1 + \Psi_1^+\underline{\mathcal{Z}}_1 - \Psi_1^-\overline{\mathcal{Z}}_1 \tag{24}$$

$$\overline{\Xi}_{\mathcal{O}1} = \mathcal{J}_1^+\overline{\Xi}_1 - \mathcal{J}_1^-\underline{\Xi}_1 \tag{25}$$

$$\underline{\Xi}_{\mathcal{O}1} = \mathcal{J}_1^+\underline{\Xi}_1 - \mathcal{J}_1^-\overline{\Xi}_1 \tag{26}$$

where $\overline{\Xi}_1$ and $\overline{\Xi}_{\mathcal{O}1}$ denote the interval upper bounds estimation value of Ξ_1 and $\Xi_{\mathcal{O}1}$, respectively. Correspondingly, the lower bounds estimation of Ξ_1 and $\Xi_{\mathcal{O}1}$ are defined as $\underline{\Xi}_1$ and $\underline{\Xi}_{\mathcal{O}1}$. The detailed adaptive laws of $\overline{\mathcal{Z}}_1$ and $\underline{\mathcal{Z}}_1$ are given below. As described in Lemma 1, $\Psi_1^+, \Psi_1^-, \mathcal{J}_1^+, \mathcal{J}_1^-$ can be calculated from Ψ_1 and $\mathcal{J}_1$.

For clarity, the dynamics of $\overline{\mathcal{Z}}_{1i}, i = 1,2,3$ and $\underline{\mathcal{Z}}_{1i}$ are designed and provided as follows

$$\dot{\overline{\mathcal{Z}}}_{1i} = \begin{cases} -\overline{\alpha_{1i}}\text{sgn}\left(\overline{\Xi}_{\mathcal{O}1i} - \Xi_{\mathcal{O}1i}\right), \\ \qquad\qquad \overline{\Xi}_{\mathcal{O}1i} - \Xi_{\mathcal{O}1i} \geq \beta_{1i} \\ \overline{\alpha_{1i}}\left|\text{sgn}\left(\overline{\Xi}_{\mathcal{O}1i} - \Xi_{\mathcal{O}1i} - \gamma_{1i}\right) - 1\right|, \\ \qquad\qquad \overline{\Xi}_{\mathcal{O}1i} - \Xi_{\mathcal{O}1i} < \beta_{1i} \end{cases} \tag{27}$$

$$\dot{\underline{\mathcal{Z}}}_{1i} = \begin{cases} \underline{\alpha_{1i}}\text{sgn}\left(\Xi_{\mathcal{O}1i} - \underline{\Xi}_{\mathcal{O}1i}\right), \\ \qquad\qquad \Xi_{\mathcal{O}1i} - \underline{\Xi}_{\mathcal{O}1i} \geq \beta_{1i} \\ -\underline{\alpha_{1i}}\left|\text{sgn}\left(\Xi_{\mathcal{O}1i} - \underline{\Xi}_{\mathcal{O}1i} - \gamma_{1i}\right) - 1\right|, \\ \qquad\qquad \Xi_{\mathcal{O}1i} - \underline{\Xi}_{\mathcal{O}1i} < \beta_{1i} \end{cases} \tag{28}$$

where $\overline{\alpha_{1i}}$, $\underline{\alpha_{1i}}$, γ_{1i}, and β_{1i} are interval observer design parameters that together determine the update and change of the interval boundaries $\overline{\mathcal{Z}}_{1i}$ and $\underline{\mathcal{Z}}_{1i}$. Moreover, these design parameters satisfy $\overline{\alpha_{1i}} > 0$, $\underline{\alpha_{1i}} > 0$, and $\beta_{1i} > \gamma_{1i} > 0$. Meanwhile, the initial values of $\overline{\mathcal{Z}}_{1i}$ and $\underline{\mathcal{Z}}_{1i}$ are subject to $\overline{\mathcal{Z}}_{1i}(0) > 0$ and $\underline{\mathcal{Z}}_{1i}(0) < 0$.

Theorem 2. *Based on the interval observer (23)–(28) designed for the Ξ_1 subsystem (20), when the position and attitude sensors are healthy, using the Luenberger observer designed in (14) and (15), there exists a finite moment t_{Ξ_1} such that the corresponding observer error Ξ_1 lies within a reasonable interval after moment t_{Ξ_1}. Moreover, the upper and lower interval boundaries $\overline{\Xi}_1, \underline{\Xi}_1, \overline{\Xi}_{\mathcal{O}1}, \underline{\Xi}_{\mathcal{O}1}, \overline{\mathcal{Z}}_1$, and $\underline{\mathcal{Z}}_1$ can be obtained by the designed interval observer (23)–(28) . Namely, $\underline{\mathcal{Z}}_1 \leq \mathcal{Z}_1 \leq \overline{\mathcal{Z}}_1$, $\underline{\Xi}_1 \leq \Xi_1 \leq \overline{\Xi}_1$, $\underline{\Xi}_{\mathcal{O}1} \leq \Xi_{\mathcal{O}1} \leq \overline{\Xi}_{\mathcal{O}1}$ hold when $t \geq t_{\Xi_1}$.*

Proof. Recalling (20), (23) and (24), it is derived that

$$\dot{\overline{\Xi}}_1 - \dot{\Xi}_1 = Y_1\left(\overline{\Xi}_1 - \Xi_1\right) + \Psi_1^+\overline{\mathcal{Z}}_1 - \Psi_1^-\underline{\mathcal{Z}}_1 - \Psi_1\mathcal{Z}_1 \tag{29}$$

$$\dot{\Xi}_1 - \dot{\underline{\Xi}}_1 = Y_1\left(\Xi_1 - \underline{\Xi}_1\right) + \Psi_1\mathcal{Z}_1 - \Psi_1^+\underline{\mathcal{Z}}_1 + \Psi_1^-\overline{\mathcal{Z}}_1 \tag{30}$$

It can be firstly proved that, by constructing the interval observer structure as in (23)–(28), the following conclusion holds

$$\underline{\mathcal{Z}}_1 \leq \mathcal{Z}_1 \leq \overline{\mathcal{Z}}_1, \text{ for } t \geq t_{\Xi_1} \tag{31}$$

If $\underline{\mathcal{Z}}_1 \leq \mathcal{Z}_1 \leq \overline{\mathcal{Z}}_1$ does not hold, then it leads to $\mathcal{Z}_{1i} < \underline{\mathcal{Z}}_{1i}$, or $\mathcal{Z}_{1i} > \overline{\mathcal{Z}}_{1i}, i = 1,2,3$. Consequently, in conjunction with (29) and (30), $\overline{\Xi}_{1i} < \Xi_{1i}$ or $\Xi_{1i} < \underline{\Xi}_{1i}$ may hold. Combining (20), (25), and (26) , we can obtain $\overline{\Xi}_{\mathcal{O}1i} < \Xi_{\mathcal{O}1i}$ or $\underline{\Xi}_{\mathcal{O}1i} > \Xi_{\mathcal{O}1i}$ in this case. It is worth noting that by devising the interval observers as in (27) and (28), the following conclusions can be derived

$$\dot{\overline{\mathcal{Z}}}_{1i} = \begin{cases} -\overline{\alpha_{1i}} < 0, & \overline{\Xi}_{\mathcal{O}1i} - \Xi_{\mathcal{O}1i} \geq \beta_{1i} \\ \overline{\alpha_{1i}} \text{ or } 2\overline{\alpha_{1i}} > 0, & \overline{\Xi}_{\mathcal{O}1i} - \Xi_{\mathcal{O}1i} \leq \gamma_{1i} \\ 0, & \gamma_{1i} < \overline{\Xi}_{\mathcal{O}1i} - \Xi_{\mathcal{O}1i} < \beta_{1i} \end{cases} \tag{32}$$

$$\dot{\underline{\mathcal{Z}}}_{1i} = \begin{cases} \underline{\alpha_{1i}} > 0, & \Xi_{\mathcal{O}1i} - \underline{\Xi}_{\mathcal{O}1i} \geq \beta_{1i} \\ -\underline{\alpha_{1i}} \text{ or } -2\underline{\alpha_{1i}} < 0, & \Xi_{\mathcal{O}1i} - \underline{\Xi}_{\mathcal{O}1i} \leq \gamma_{1i} \\ 0, & \gamma_{1i} < \Xi_{\mathcal{O}1i} - \underline{\Xi}_{\mathcal{O}1i} < \beta_{1i} \end{cases} \tag{33}$$

With the aid of the properties of (32) and (33), it follows that $\dot{\overline{\mathcal{Z}}}_{1i} > 0$ or $\dot{\underline{\mathcal{Z}}}_{1i} < 0$ when $\mathcal{Z}_{1i} > \overline{\mathcal{Z}}_{1i}$ or $\mathcal{Z}_{1i} < \underline{\mathcal{Z}}_{1i}$, thus there exists a finite moment $t_{\Xi_{1i}}$ such that $\underline{\mathcal{Z}}_{1i} \leq \mathcal{Z}_{1i} \leq \overline{\mathcal{Z}}_{1i}$ holds for $t \geq t_{\Xi_{1i}}$. Let $t_{\Xi_1} = \max\{t_{\Xi_{1i}}, i = 1,2,3\}$, we can obtain (31). When $\underline{\mathcal{Z}}_1 \leq \mathcal{Z}_1 \leq \overline{\mathcal{Z}}_1$, combining Lemma 1, we can get

$$\Psi_1^+\overline{\mathcal{Z}}_1 - \Psi_1^-\underline{\mathcal{Z}}_1 - \Psi_1\mathcal{Z}_1 \geq 0 \tag{34}$$

$$\Psi_1\mathcal{Z}_1 - \Psi_1^+\underline{\mathcal{Z}}_1 + \Psi_1^-\overline{\mathcal{Z}}_1 \geq 0 \tag{35}$$

It is straightforward to observe that Y_1 is a Metzler matrix. By invoking Lemma 2, when $t \geq t_{\Xi_1}$, we can obtain

$$\underline{\Xi}_1 \leq \Xi_1 \leq \overline{\Xi}_1 \tag{36}$$

$$\underline{\Xi}_{\mathcal{O}1} \le \Xi_{\mathcal{O}1} \le \overline{\Xi}_{\mathcal{O}1} \tag{37}$$

The proof of Theorem 2 is completed. ■

Similar to the Ξ_1 subsystem (20), an interval observer is designed for the Ξ_2 subsystem (21) to estimate the interval upper and lower bounds $\overline{\Xi}_1, \underline{\Xi}_1, \overline{\Xi}_{\mathcal{O}2}$ and $\underline{\Xi}_{\mathcal{O}2}$ of Ξ_2 and $\Xi_{\mathcal{O}2}$. The detailed interval observer design for Ξ_2 subsystem (21) is provided below. Specifically, $\overline{\Xi}_{\mathcal{O}2}$, $\underline{\Xi}_{\mathcal{O}2}$ and the derivatives of $\overline{\Xi}_2$ and $\underline{\Xi}_2$ can be calculated by

$$\dot{\overline{\Xi}}_2 = Y_2\overline{\Xi}_2 + \Psi_2^+\overline{\mathcal{Z}}_2 - \Psi_2^-\underline{\mathcal{Z}}_2 \tag{38}$$

$$\dot{\underline{\Xi}}_2 = Y_2\underline{\Xi}_2 + \Psi_2^+\underline{\mathcal{Z}}_2 - \Psi_2^-\overline{\mathcal{Z}}_2 \tag{39}$$

$$\overline{\Xi}_{\mathcal{O}2} = \mathcal{J}_2^+\overline{\Xi}_2 - \mathcal{J}_2^-\underline{\Xi}_2 \tag{40}$$

$$\underline{\Xi}_{\mathcal{O}2} = \mathcal{J}_2^+\underline{\Xi}_2 - \mathcal{J}_2^-\overline{\Xi}_2 \tag{41}$$

where $\Psi_2^+, \Psi_2^-, \mathcal{J}_2^+, \mathcal{J}_2^-$ can be obtained as defined in Lemma 1. Moreover, the derivatives of $\overline{\mathcal{Z}}_2$ and $\underline{\mathcal{Z}}_2$ are designed and given detailedly as

$$\dot{\overline{\mathcal{Z}}}_{2i} = \begin{cases} -\overline{\alpha_{2i}}\,\mathrm{sgn}\left(\overline{\Xi}_{\mathcal{O}2i} - \Xi_{\mathcal{O}2i}\right), \\ \qquad\qquad \overline{\Xi}_{\mathcal{O}2i} - \Xi_{\mathcal{O}2i} \ge \beta_{2i} \\ \overline{\alpha_{2i}}\left|\mathrm{sgn}\left(\overline{\Xi}_{\mathcal{O}2i} - \Xi_{\mathcal{O}2i} - \gamma_{2i}\right) - 1\right|, \\ \qquad\qquad \overline{\Xi}_{\mathcal{O}2i} - \Xi_{\mathcal{O}2i} < \beta_{2i} \end{cases} \tag{42}$$

$$\dot{\underline{\mathcal{Z}}}_{2i} = \begin{cases} \underline{\alpha_{2i}}\,\mathrm{sgn}\left(\Xi_{\mathcal{O}2i} - \underline{\Xi}_{\mathcal{O}2i}\right), \\ \qquad\qquad \Xi_{\mathcal{O}2i} - \underline{\Xi}_{\mathcal{O}2i} \ge \beta_{2i} \\ -\underline{\alpha_{2i}}\left|\mathrm{sgn}\left(\Xi_{\mathcal{O}2i} - \underline{\Xi}_{\mathcal{O}2i} - \gamma_{2i}\right) - 1\right|, \\ \qquad\qquad \Xi_{\mathcal{O}2i} - \underline{\Xi}_{\mathcal{O}2i} < \beta_{2i} \end{cases} \tag{43}$$

where $\overline{\alpha_{2i}}$, $\underline{\alpha_{2i}}$, β_{2i}, and γ_{2i} are the artificially given interval observer parameters that satisfying $\overline{\alpha_{2i}} > 0, \underline{\alpha_{2i}} > 0$, and $\beta_{2i} > \gamma_{2i} > 0$. Meanwhile, the initial estimation values of the upper and lower bounds $\overline{\mathcal{Z}}_2$ and $\underline{\mathcal{Z}}_2$ satisfy $\overline{\mathcal{Z}}_2(0) > 0$ and $\underline{\mathcal{Z}}_2(0) < 0$.

Theorem 3. *The upper and lower bounds on the interval of Ξ_2 and $\Xi_{\mathcal{O}2}$ without sensor faults can be effectively estimated by using interval observer (38)–(43) for the subsystem ((21)). As proved above, employing the Luenberger observer constructed in (14) and (15) with reasonable observer parameters setting, the estimation errors Ξ_2 and $\Xi_{\mathcal{O}2}$ are bounded and within an interval, when sensor faults are free. The interval upper and lower bounds $\overline{\Xi}_{\mathcal{O}2}$ and $\underline{\Xi}_{\mathcal{O}2}$ can be obtained adaptively in a finite time t_{Ξ_2} by using the designed adaptive update laws (38)–(43). That is, for $t \ge t_{\Xi_2}$, $\underline{\mathcal{Z}}_2 \le \mathcal{Z}_2 \le \overline{\mathcal{Z}}_2$, $\underline{\Xi}_2 \le \Xi_2 \le \overline{\Xi}_2$, and $\underline{\Xi}_{\mathcal{O}2} \le \Xi_{\mathcal{O}2} \le \overline{\Xi}_{\mathcal{O}2}$ hold.*

Proof. Based on (21) and the designed interval observer adaptive update laws (38) and (39), we can derive

$$\dot{\overline{\Xi}}_2 - \dot{\Xi}_2 = Y_2\left(\overline{\Xi}_2 - \Xi_2\right) + \Psi_2^+\overline{\mathcal{Z}}_2 - \Psi_2^-\underline{\mathcal{Z}}_2 - \Psi_2\mathcal{Z}_2 \tag{44}$$

$$\dot{\Xi}_2 - \dot{\underline{\Xi}}_2 = Y_2\left(\Xi_2 - \underline{\Xi}_2\right) + \Psi_2\mathcal{Z}_2 - \Psi_2^+\underline{\mathcal{Z}}_2 + \Psi_2^-\overline{\mathcal{Z}}_2 \tag{45}$$

According to the interval observer constructed in (42) and (43), it is obvious that the dynamics $\dot{\overline{\mathcal{Z}}}_{2i}$ and $\dot{\underline{\mathcal{Z}}}_{2i}$ have the following properties

$$\dot{\overline{\mathcal{Z}}}_{2i} = \begin{cases} -\overline{\alpha_{2i}} < 0, & \overline{\Xi}_{\mathcal{O}2i} - \Xi_{\mathcal{O}2i} \ge \beta_{2i} \\ \overline{\alpha_{2i}} \text{ or } 2\overline{\alpha_{2i}} > 0, & \overline{\Xi}_{\mathcal{O}2i} - \Xi_{\mathcal{O}2i} \le \gamma_{2i} \\ 0, & \gamma_{2i} < \overline{\Xi}_{\mathcal{O}2i} - \Xi_{\mathcal{O}2i} < \beta_{2i} \end{cases} \tag{46}$$

$$\dot{\underline{\mathcal{Z}}}_{2i} = \begin{cases} \underline{\alpha_{2i}} > 0, & \Xi_{\mathcal{O}2i} - \underline{\Xi}_{\mathcal{O}2i} \ge \beta_{2i} \\ -\underline{\alpha_{2i}} \text{ or } -2\underline{\alpha_{2i}} < 0, & \Xi_{\mathcal{O}2i} - \underline{\Xi}_{\mathcal{O}2i} \le \gamma_{2i} \\ 0, & \gamma_{2i} < \Xi_{\mathcal{O}2i} - \underline{\Xi}_{\mathcal{O}2i} < \beta_{2i} \end{cases} \tag{47}$$

Similar to the analysis and proof of Theorem 2, we have the following conclusion

$$\underline{\mathcal{Z}}_2 \le \mathcal{Z}_2 \le \overline{\mathcal{Z}}_2, \text{ for } t \ge t_{\Xi_2} \tag{48}$$

By using Lemma 1, we have

$$\Psi_2^+\overline{\mathcal{Z}}_2 - \Psi_2^-\underline{\mathcal{Z}}_2 - \Psi_2\mathcal{Z}_2 \ge 0 \tag{49}$$

$$\Psi_2\mathcal{Z}_2 - \Psi_2^+\underline{\mathcal{Z}}_2 + \Psi_2^-\overline{\mathcal{Z}}_2 \ge 0 \tag{50}$$

Meanwhile, according to Lemma 2, we can get

$$\underline{\Xi}_2 \le \Xi_2 \le \overline{\Xi}_2 \tag{51}$$

$$\underline{\Xi}_{\mathcal{O}2} \le \Xi_{\mathcal{O}2} \le \overline{\Xi}_{\mathcal{O}2} \tag{52}$$

hold for $t \ge t_{\Xi_2}$, thus completing the proof of Theorem 3. ■

3.2. Sensor fault detection and isolation

By utilizing the developed interval observers (23)–(28) and (38)–(43), the sensor faults can be detected and isolated effectively. In this paper, it is assumed that only one sensor fault occurs at once. In essential, when sensor faults are free, the constructed Luenberger observer and interval observer enable $\Xi_{\mathcal{O}1}$ and $\Xi_{\mathcal{O}2}$ within the interval $(\underline{\Xi}_{\mathcal{O}1}, \overline{\Xi}_{\mathcal{O}1})$ and $(\underline{\Xi}_{\mathcal{O}2}, \overline{\Xi}_{\mathcal{O}2})$ after moment $t_\Xi = \max\{t_{\Xi_1}, t_{\Xi_2}\}$. However, $\Xi_{\mathcal{O}1i}$ or $\Xi_{\mathcal{O}2i}$ may exceed the corresponding estimation interval when a sensor fault occurs which is used to detect and isolate the fault. Specifically, from (10), the sensor fault model considered in this paper can be expressed as

$$\mathcal{O}_{ij} = \mathcal{E}_{ij} + S_{ij} \tag{53}$$

where $i = 1, 2$ and $j = 1, 2, 3$. S_{ij} denotes the occurred sensor fault, and $S_{ij} = 0$ means that the corresponding sensor is fault-free. Accordingly, when the sensor is healthy, $\Xi_{\mathcal{O}1i}$, $\Xi_{\mathcal{O}2i}$ and the dynamics of Ξ_{1i}, Ξ_{2i} are consistent with (20) and (21), namely

$$\dot{\Xi}_{ij} = Y_{ij}\Xi_{ij} + \Psi_{ij}\mathcal{Z}_{ij}, \Xi_{\mathcal{O}ij} = \mathcal{J}_{ij}\Xi_{ij} \tag{54}$$

Define $\mathcal{G}_i := -C_i, i = 1, 2$, $\dot{\Xi}_{ij}$ and $\Xi_{\mathcal{O}ij}$ with sensor fault can be written as

$$\dot{\Xi}_{ij} = Y_{ij}\Xi_{ij} + \Psi_{ij}\mathcal{Z}_{ij} + \mathcal{G}_{ij}S_{ij} \tag{55}$$

$$\Xi_{\mathcal{O}ij} = \mathcal{J}_{ij}\Xi_{ij} + S_{ij} \tag{56}$$

where $\mathcal{G}_{ij}$ represents the jth element on the diagonal.

By employing the designed Luenberger observer and interval observers, the following cases are possible

(a) After finite time $t_{\Xi_{ij}}$, as proved in Theorems 2 and 3, $\Xi_{\mathcal{O}ij}$ enters the corresponding estimation interval. Namely, $\underline{\Xi}_{\mathcal{O}ij} \le \Xi_{\mathcal{O}ij} \le \overline{\Xi}_{\mathcal{O}ij}$ hold, when $t \ge t_{\Xi_{ij}}$.

(b) There exists a moment $t_{\mathcal{H}_{ij}}$, when $t \ge t_{\mathcal{H}_{ij}} \ge t_{\mathcal{R}_{ij}} \ge t_{\Xi_{ij}}$, $\Xi_{\mathcal{O}ij}$ in the $\mathcal{O}_i$ subsystem exceed the estimation interval $[\underline{\Xi}_{\mathcal{O}ij}, \overline{\Xi}_{\mathcal{O}ij}]$ caused by the occurred sensor fault. And $t_{\mathcal{R}_{ij}}$ represents the moment when the sensor fault occurs. It means that, when $t \in [t_{\Xi_{ij}}, t_{\mathcal{H}_{ij}}]$, we have $\Xi_{\mathcal{O}ij} \in [\underline{\Xi}_{\mathcal{O}ij}, \overline{\Xi}_{\mathcal{O}ij}]$. When $t \ge t_{\mathcal{H}_{ij}}$, there is either $\Xi_{\mathcal{O}ij} > \overline{\Xi}_{\mathcal{O}ij}$ or $\Xi_{\mathcal{O}ij} < \underline{\Xi}_{\mathcal{O}ij}$.

(c) $\Xi_{\mathcal{O}ij}$ cannot enter the corresponding estimation interval $[\underline{\Xi}_{\mathcal{O}ij}, \overline{\Xi}_{\mathcal{O}ij}]$, that is, for $t \ge 0$, $\Xi_{\mathcal{O}ij} \notin [\underline{\Xi}_{\mathcal{O}ij}, \overline{\Xi}_{\mathcal{O}ij}]$.

According to the above cases, we can detect and isolate the sensor fault accordingly. The specific principles are detailed as follows

- Case (a) indicates that the corresponding sensor is healthy. If case (a) holds, for $i = 1, 2$, $j = 1, 2, 3$, it means that all sensors are fault-free.
- For Case (b), it means that a fault occurs in the corresponding sensor. The fault occurrence time is $t_{\mathcal{H}_{ij}}$. $i = 1$, $j = 1$ or 2 indicates the corresponding position sensor is faulty. $i = 1$, $j = 3$ means that the vehicle attitude sensor is unhealthy. $i = 2$, $j = 1, 2$ or 3 indicates that the corresponding speed sensor is faulty. Thus, the sensor fault occurrence time and location can be detected and isolated as above.

- Similar to the description for Case (b), we consider that for $t \geq 0$, the corresponding sensor is faulty for Case (c).

Remark 2. Sensor faults are generally more serious and difficult to deal with than actuator faults (Wang & Xiao, 2004). Sensor fault detection and isolation are essential to ensure the reliability and safety of vehicle systems. Fault detection (He, Wang, & Zhou, 2009; Ji, He, Shang, & Zhou, 2017) can provide users with fault warnings. However, intelligent vehicles are equipped with a multitude of sensors to monitor vehicle states. Thus, pinpointing faulty sensor location through fault isolation can aid in timely addressing the occurred fault. Combined with the sensor fault model (53), it can be seen that employing the fault detection and isolation mechanisms designed above can detect faults that occur and determine which vehicle position or velocity sensor is faulty. Fault location information can help estimate the occurred fault from a software perspective or replace the faulty sensor promptly to mitigate or avoid potential adverse effects.

3.3. Sensor fault estimation

When the corresponding sensor fault is detected, the fault estimation can be calculated by modifying the designed interval observer. As detailed above, the corresponding observer structure for a healthy sensor remains unchanged. Meanwhile, to estimate the sensor fault, the corresponding modified interval observer is provided as follows

$$\dot{\overline{\Xi}}_{ij} = Y_{ij}\overline{\Xi}_{ij} + \Psi_{ij}^{+}\overline{\mathcal{Z}}_{ij} - \Psi_{ij}^{-}\underline{\mathcal{Z}}_{ij} + \mathcal{G}_{ij}^{+}\overline{S}_{ij} - \mathcal{G}_{ij}^{-}\underline{S}_{ij} \tag{57}$$

$$\dot{\underline{\Xi}}_{ij} = Y_{ij}\underline{\Xi}_{ij} + \Psi_{ij}^{+}\underline{\mathcal{Z}}_{ij} - \Psi_{ij}^{-}\overline{\mathcal{Z}}_{ij} + \mathcal{G}_{ij}^{+}\underline{S}_{ij} - \mathcal{G}_{ij}^{-}\overline{S}_{ij} \tag{58}$$

$$\overline{\Xi}_{\mathcal{O}ij} = \mathcal{J}_{ij}^{+}\overline{\Xi}_{ij} - \mathcal{J}_{ij}^{-}\underline{\Xi}_{ij} + \overline{S}_{ij} \tag{59}$$

$$\underline{\Xi}_{\mathcal{O}ij} = \mathcal{J}_{ij}^{+}\underline{\Xi}_{ij} - \mathcal{J}_{ij}^{-}\overline{\Xi}_{ij} + \underline{S}_{ij} \tag{60}$$

The adaptive dynamics of $\overline{\mathcal{Z}}_{ij}$ and $\underline{\mathcal{Z}}_{ij}$ are given as

$$\dot{\overline{\mathcal{Z}}}_{ij} = \begin{cases} -\overline{\alpha_{ij}}\,\mathrm{sgn}\left(\overline{\Xi}_{\mathcal{O}ij} - \Xi_{\mathcal{O}ij}\right), \\ \qquad\qquad \overline{\Xi}_{\mathcal{O}ij} - \Xi_{\mathcal{O}ij} \geq \beta_{ij} \\ \overline{\alpha_{ij}}\left|\mathrm{sgn}\left(\overline{\Xi}_{\mathcal{O}ij} - \Xi_{\mathcal{O}ij} - \gamma_{ij}\right) - 1\right|, \\ \qquad\qquad \overline{\Xi}_{\mathcal{O}ij} - \Xi_{\mathcal{O}ij} < \beta_{ij} \end{cases} \tag{61}$$

$$\dot{\underline{\mathcal{Z}}}_{ij} = \begin{cases} \underline{\alpha_{ij}}\,\mathrm{sgn}\left(\Xi_{\mathcal{O}ij} - \underline{\Xi}_{\mathcal{O}ij}\right), \\ \qquad\qquad \Xi_{\mathcal{O}ij} - \underline{\Xi}_{\mathcal{O}ij} \geq \beta_{ij} \\ -\underline{\alpha_{ij}}\left|\mathrm{sgn}\left(\Xi_{\mathcal{O}2i} - \underline{\Xi}_{\mathcal{O}2i} - \gamma_{ij}\right) - 1\right|, \\ \qquad\qquad \Xi_{\mathcal{O}ij} - \underline{\Xi}_{\mathcal{O}ij} < \beta_{ij} \end{cases} \tag{62}$$

where $\overline{\alpha_{ij}} \in \mathbb{R}^{+}, \underline{\alpha_{ij}} \in \mathbb{R}^{+}$, and $\beta_{ij} > \gamma_{ij} > 0$ are the tunable observer parameters.

Moreover, by selecting the observer parameters $\overline{\mu_{ij}} \in \mathbb{R}^{+}, \underline{\mu_{ij}} \in \mathbb{R}^{+}, \rho_{ij} > \ell_{ij} > 0$, the interval bounds $\underline{S}_{ij}, \overline{S}_{ij}$ of the sensor fault S_{ij} can be calculated as below

$$\dot{\overline{S}}_{ij} = \begin{cases} -\overline{\mu_{ij}}\,\mathrm{sgn}\left(\overline{\Xi}_{\mathcal{O}ij} - \Xi_{\mathcal{O}ij}\right), \\ \qquad\qquad \overline{\Xi}_{\mathcal{O}ij} - \Xi_{\mathcal{O}ij} \geq \rho_{ij} \\ \overline{\mu_{ij}}\left|\mathrm{sgn}\left(\overline{\Xi}_{\mathcal{O}ij} - \Xi_{\mathcal{O}ij} - \ell_{ij}\right) - 1\right|, \\ \qquad\qquad \overline{\Xi}_{\mathcal{O}ij} - \Xi_{\mathcal{O}ij} < \rho_{ij} \end{cases} \tag{63}$$

$$\dot{\underline{S}}_{ij} = \begin{cases} \underline{\mu_{ij}}\,\mathrm{sgn}\left(\Xi_{\mathcal{O}ij} - \underline{\Xi}_{\mathcal{O}ij}\right), \\ \qquad\qquad \Xi_{\mathcal{O}ij} - \underline{\Xi}_{\mathcal{O}ij} \geq \rho_{ij} \\ -\underline{\mu_{ij}}\left|\mathrm{sgn}\left(\Xi_{\mathcal{O}ij} - \underline{\Xi}_{\mathcal{O}ij} - \ell_{ij}\right) - 1\right|, \\ \qquad\qquad \Xi_{\mathcal{O}ij} - \underline{\Xi}_{\mathcal{O}ij} < \rho_{ij} \end{cases} \tag{64}$$

Theorem 4. *By using the modified interval observer (60)–(64), $\mathcal{Z}_{ij}$ and $\Xi_{\mathcal{O}ij}$ with sensor fault can enter the corresponding estimation interval in a finite time t_{Ξ_S}. Meanwhile, the reconstructed observer (63) and (64) can effectively estimate the upper and lower interval bounds of sensor fault S_{ij}. Namely, for $t \geq t_{\Xi_2}$, $\underline{\Xi}_{\mathcal{O}ij} \leq \Xi_{\mathcal{O}ij} \leq \overline{\Xi}_{\mathcal{O}ij}$ and $\underline{S}_{ij} \leq S_{ij} \leq \overline{S}_{ij}$ hold.*

Proof. Combining (57)–(60) and sensor faults (55)–(56) , we can get

$$\begin{aligned} \dot{\overline{\Xi}}_{ij} - \dot{\Xi}_{ij} =& Y_{ij}\left(\overline{\Xi}_{ij} - \Xi_{ij}\right) + \Psi_2^{+}\overline{\mathcal{Z}}_{ij} - \Psi_2^{-}\underline{\mathcal{Z}}_{ij} - \Psi_{ij}\mathcal{Z}_{ij} \\ &+ \mathcal{G}_{ij}^{+}\overline{S}_{ij} - \mathcal{G}_{ij}^{-}\underline{S}_{ij} - \mathcal{G}_{ij}S_{ij} \end{aligned} \tag{65}$$

$$\begin{aligned} \dot{\Xi}_{ij} - \dot{\underline{\Xi}}_{ij} =& Y_{ij}\left(\Xi_{ij} - \underline{\Xi}_{ij}\right) + \Psi_{ij}\mathcal{Z}_{ij} - \Psi_2^{+}\underline{\mathcal{Z}}_{ij} + \Psi_2^{-}\overline{\mathcal{Z}}_{ij} \\ &+ \mathcal{G}_{ij}S_{ij} - \left(\mathcal{G}_{ij}^{+}\underline{S}_{ij} - \mathcal{G}_{ij}^{-}\overline{S}_{ij}\right) \end{aligned} \tag{66}$$

Meanwhile, according to the designed adaptive laws (63)–(64), we can derive

$$\dot{\overline{S}}_{ij} = \begin{cases} -\overline{\mu_{ij}} < 0, & \overline{\Xi}_{\mathcal{O}ij} - \Xi_{\mathcal{O}ij} \geq \rho_{ij} \\ \overline{\mu_{ij}} \text{ or } 2\overline{\mu_{ij}} > 0, & \overline{\Xi}_{\mathcal{O}ij} - \Xi_{\mathcal{O}ij} \leq \ell_{ij} \\ 0, & \ell_{ij} < \overline{\Xi}_{\mathcal{O}ij} - \Xi_{\mathcal{O}ij} < \rho_{ij} \end{cases} \tag{67}$$

$$\dot{\underline{S}}_{ij} = \begin{cases} \underline{\mu_{ij}} > 0, & \Xi_{\mathcal{O}ij} - \underline{\Xi}_{\mathcal{O}ij} \geq \rho_{ij} \\ -\underline{\mu_{ij}} \text{ or } -2\underline{\mu_{ij}} < 0, & \Xi_{\mathcal{O}ij} - \underline{\Xi}_{\mathcal{O}ij} \leq \ell_{ij} \\ 0, & \ell_{ij} < \Xi_{\mathcal{O}ij} - \underline{\Xi}_{\mathcal{O}ij} < \rho_{ij} \end{cases} \tag{68}$$

Similar to the analysis and proof of Theorems 2 and 3, combining (65)–(68), we can prove $\Xi_{\mathcal{O}ij} \in [\underline{\Xi}_{\mathcal{O}ij}, \overline{\Xi}_{\mathcal{O}ij}]$ and $S_{ij} \in [\underline{S}_{ij}, \overline{S}_{ij}]$ hold, for $t \geq t_{\Xi_S}$. ■

Remark 3. To enhance clarity and assist users in selecting parameters, the impact of the key parameters in the proposed fault diagnosis framework is summarized. The Luenberger observer gains $C_i, i = 1, 2$ subject to $C_i > 0$, which directly determines the convergence performance of the observation errors $\Xi_i, i = 1, 2$ as detailed in Theorem 1. The interval observer parameters $\beta_{ij}, \gamma_{ij}, \rho_{ij}, \ell_{ij} \in \mathbb{R}^{+}, i = 1, 2, j = 1, 2, 3$ subject to $\beta_{ij} > \gamma_{ij}, \rho_{ij} > \ell_{ij}$ affect the corresponding interval width. Compared to the conventional interval observer (Zhang & Yang, 2017), more compact interval estimations can be obtained using the proposed adaptive update laws. And the update rates of the interval boundary estimations are directly influenced by parameters $\overline{\alpha_{ij}}, \underline{\alpha_{ij}}, \overline{\mu_{ij}}, \underline{\mu_{ij}} \in \mathbb{R}^{+}$. Opting for larger $\overline{\alpha_{ij}}, \underline{\alpha_{ij}}, \overline{\mu_{ij}}, \underline{\mu_{ij}}$ enables the bounds estimation to be updated more swiftly. Conversely, selecting smaller $\overline{\alpha_{ij}}, \underline{\alpha_{ij}}, \overline{\mu_{ij}}, \underline{\mu_{ij}}$ yields finer bounds estimations. The parameters of the observer need to be carefully adjusted and customized by users to satisfy specific requirements. The performance influences of the main sensitive parameters are summarized above. For different fault scenarios, further adjustments may be required to change the parameters to achieve satisfactory performance.

4. Simulation results

In order to validate the proposed sensor fault detection, isolation, and estimation framework, simulation results based on the J-Turn scenario are provided in this section. The definition of parameters in this section remains the same as in Section 3, with the same letters or symbols having the same meaning. In practice, the parameters can be adjusted in conjunction with the analysis in Remark 3 until satisfactory performance is achieved. The effectiveness of the Luenberger observer (14)–(15) and the interval observers (23)–(26) and (38)–(41) designed for Ξ_1 and Ξ_2 subsystems can be proved by the simulation results. Meanwhile, it can be observed that the designed fault detection and isolation framework can detect sensor faults and isolate the faulty sensor efficiently. Further, the modified interval observer can achieve an effective estimation of the upper and lower interval bounds of the sensor fault.

The J-Turn condition (Zhang et al., 2019) as the standard test condition for vehicles is used in this paper as the simulation test

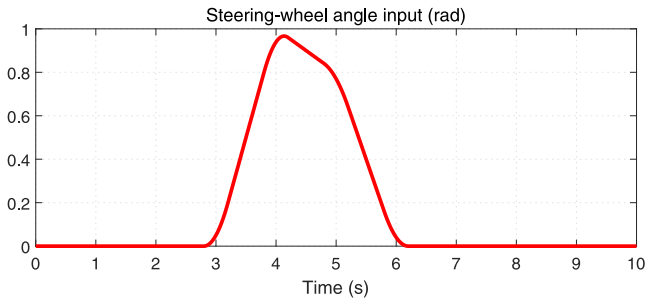

Fig. 2. Steering-wheel angle input for J-Turn scenario.

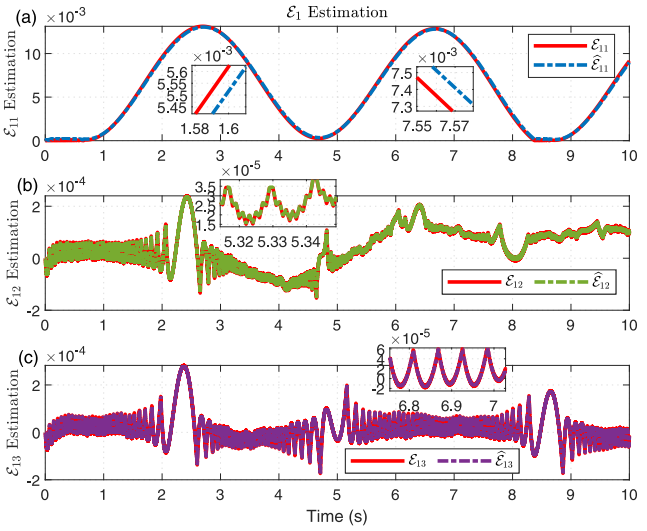

Fig. 3. $\mathcal{E}_1$ estimation for S1.

scenario. The steering wheel angle input for the J-Turn (Zhang et al., 2019) simulation scenario is plotted in Fig. 2. The longitudinal desired time-varying velocity is set to $10 + sin(0.5\pi t)$. White Gaussian noises with a power equal to 0.1 are added to vehicle sensors. The corresponding reference trajectory can be calculated by the reference value generation method in Zhang et al. (2019). The calculated desired trajectory is tracked by the sliding mode controller in (22) with the controller gains $\mathcal{K}_1 = \text{diag}(210, 13, 10)$ and $\mathcal{K}_d = \text{diag}(10, 10, 10)$. To evaluate the proposed sensor fault detection, isolation, and estimation scheme, simulation results of the following scenarios are provided: S1: sensor fault-free scenario; S2: occurred a sensor fault; S3: sensor fault estimation with a modified interval observer structure; S4: comparative results with existing methods.

4.1. S1

The Luenberger observer parameters are chosen as C_1 :=diag(10, 1100, 1400) and C_2 :=diag(54, 1000, 1800). The interval observer parameters designed for the Ξ_1 and Ξ_2 subsystems are set as $\overline{\alpha_{11}} = 1$, $\underline{\alpha_{11}} = 10$, $\gamma_{11} = 10^{-3}$, $\beta_{11} = 10$, $\overline{\alpha_{12}} = 0.01$, $\underline{\alpha_{12}} = 0.01$, $\gamma_{12} = 10^{-5}$, $\beta_{12} = 10^{-3}$, $\overline{\alpha_{13}} = 0.01$, $\underline{\alpha_{13}} = 0.01$, $\gamma_{13} = 10^{-5}$, $\beta_{13} = 10^{-3}$, $\overline{\alpha_{21}} = 0.5$, $\underline{\alpha_{21}} = 0.01$, $\beta_{21} = 5 * 10^{-3}$, $\gamma_{21} = 2 * 10^{-4}$, $\overline{\alpha_{22}} = 1$, $\underline{\alpha_{22}} = 50$, $\beta_{22} = 2 * 10^{-3}$, $\gamma_{22} = 5 * 10^{-4}$, $\overline{\alpha_{23}} = 20$, $\underline{\alpha_{23}} = 10$, $\beta_{23} = 5 * 10^{-3}$, and $\gamma_{23} = 1 * 10^{-4}$.

The observer structure (14) with the chosen parameters enables an accurate estimation of the system state $\mathcal{E}_1$ in (8). The initial values of the observer estimations for $\hat{\mathcal{E}}_1$ and $\hat{\mathcal{E}}_2$ are $\hat{\mathcal{E}}_1(0) = [0, 0, 0]^T$ and $\hat{\mathcal{E}}_2(0) = [0, 0, 0]^T$. Specifically, the estimations for $\mathcal{E}_{11}$, $\mathcal{E}_{12}$, and $\mathcal{E}_{13}$ for S1 are shown in Fig. 3(a), (b) and (c), respectively. It can be seen that

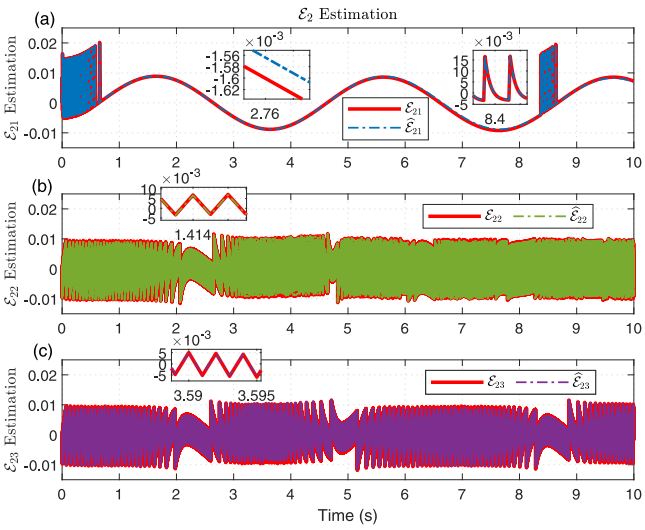

Fig. 4. $\mathcal{E}_2$ estimation for S1.

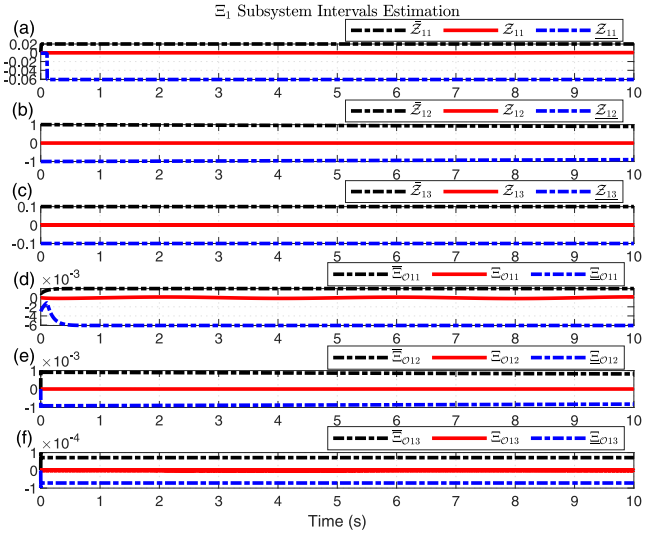

Fig. 5. Ξ_1 subsystem intervals estimation for S1.

accurate estimations of the $\mathcal{E}_1$ subsystem states can be achieved by the designed Luenberger observer (14).

Also, the estimation and corresponding actual state for $\mathcal{E}_2$ is illustrated in Fig. 4. As can be seen in Fig. 4(a), (b), and (c), accurate estimation of $\mathcal{E}_{21}$, $\mathcal{E}_{22}$, and $\mathcal{E}_{23}$ can be achieved by selecting observer gains carefully. The effectiveness of the designed observer can be demonstrated by the estimation results in Figs. 3 and 4. The real-time state accurate observation can be further seen from the local zoom in the figures. It is clear that using the designed states observer (14) and (15) with reasonable observer gains that can achieve efficient estimations of the system states $\mathcal{E}_1$ and $\mathcal{E}_2$.

As depicted in Figs. 5–7, the upper and lower interval bounds of the corresponding variables $\mathcal{Z}_1$, $\mathcal{Z}_2$, $\Xi_{\mathcal{O}1}$ and $\Xi_{\mathcal{O}2}$ in subsystems Ξ_1 and Ξ_2 can be estimated adaptively by employing the designed interval observers (23)–(28) and (38)–(43). By adaptive updating, the corresponding states enter the interval with the estimated bounds. The initial values of the interval estimations are $\underline{\mathcal{Z}}_1(0) = [-10^{-3}, -1, -0.1]^T$, $\overline{\mathcal{Z}}_1(0) = [10^{-3}, 1, 0.1]^T$, $\overline{\Xi}_1 = [10^{-3}, 10^{-5}, 10^{-5}]^T$, $\underline{\Xi}_{\mathcal{O}1} = [-10^{-3}, -10^{-3}, -10^{-3}]^T$, $\overline{\Xi}_{\mathcal{O}1} = [10^{-3}, 10^{-3}, 10^{-3}]^T$, and $\underline{\Xi}_1 = [-3 * 10^{-3}, -10^{-5}, -10^{-5}]^T$. In specific, for the Ξ_1 subsystem, it can be seen from Fig. 5(a), (b) and (c)

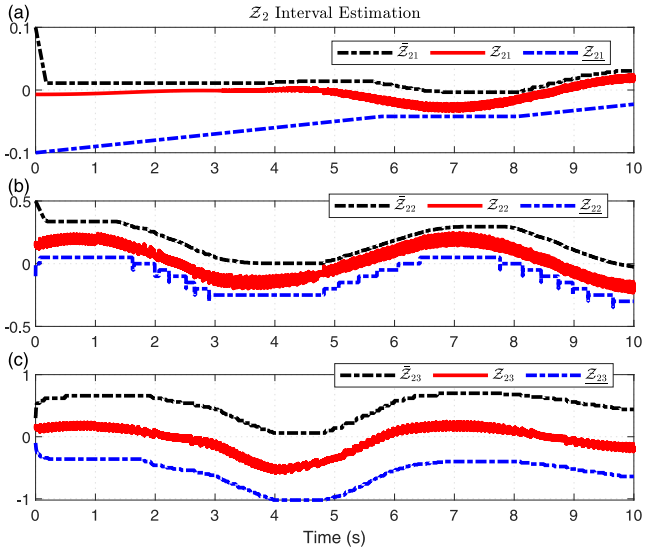

Fig. 6. $\mathcal{Z}_2$ interval estimation for S1.

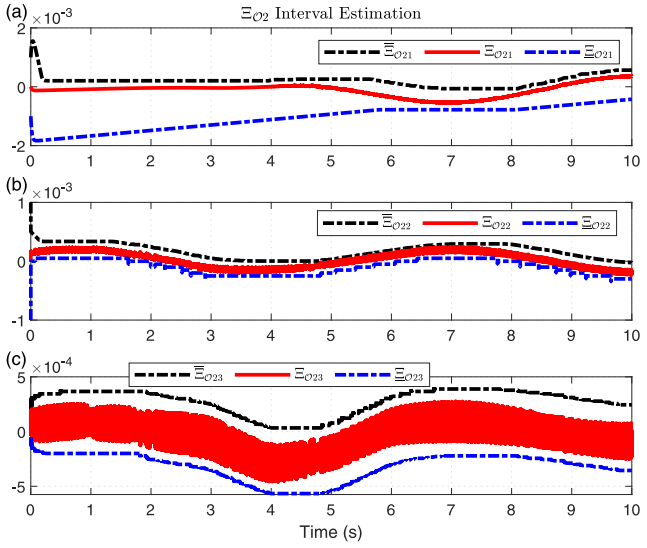

Fig. 7. $\Xi_{\mathcal{O}2}$ interval estimation for S1.

that $\underline{\Xi}_1 \le \Xi_1 \le \overline{\Xi}_1$ holds by using the constructed adaptive estimation laws and $\underline{\Xi}_{\mathcal{O}1} \le \Xi_{\mathcal{O}1} \le \overline{\Xi}_{\mathcal{O}1}$ satisfies as in Fig. 5(d), (e), and (f).

Meanwhile, the variables $\mathcal{Z}_2$ and $\Xi_{\mathcal{O}2}$ in the Ξ_2 subsystem can enter into the corresponding estimation interval $[\underline{\mathcal{Z}}_2, \overline{\mathcal{Z}}_2]$ and $[\underline{\Xi}_{\mathcal{O}2}, \overline{\Xi}_{\mathcal{O}2}]$ by employing the observer structures (38)–(43), as in Figs. 6 and 7. The initial values of the interval estimations in the Ξ_2 subsystem are $\underline{\mathcal{Z}}_1(0) = [-10^{-3}, -1, -0.1]^T$, $\overline{\mathcal{Z}}_1(0) = [10^{-3}, 1, 0.1]^T$, $\overline{\Xi}_1 = [10^{-3}, 10^{-5}, 10^{-5}]^T$, $\underline{\Xi}_{\mathcal{O}1} = [-10^{-3}, -10^{-3}, -10^{-3}]^T$, $\overline{\Xi}_{\mathcal{O}1} = [10^{-3}, 10^{-3}, 10^{-3}]^T$, and $\underline{\Xi}_1 = [-3 * 10^{-3}, -10^{-5}, -10^{-5}]^T$. It is worth noting that for vehicle-integrated motion systems (8) and (9) with external perturbations and uncertainties, $\underline{\mathcal{Z}}_2$, $\overline{\mathcal{Z}}_2$, $\underline{\Xi}_{\mathcal{O}2}$, and $\overline{\Xi}_{\mathcal{O}2}$ can be estimated adaptively using the presented method. The constructed observer structure is simple and effective. As illustrated in Fig. 6 and 7, the interval bounds are real-time adaptively updated allowing us to obtain the interval upper and lower bounds $\underline{\mathcal{Z}}_2$, $\overline{\mathcal{Z}}_2$, $\underline{\Xi}_{\mathcal{O}2}$, and $\overline{\Xi}_{\mathcal{O}2}$ efficiently.

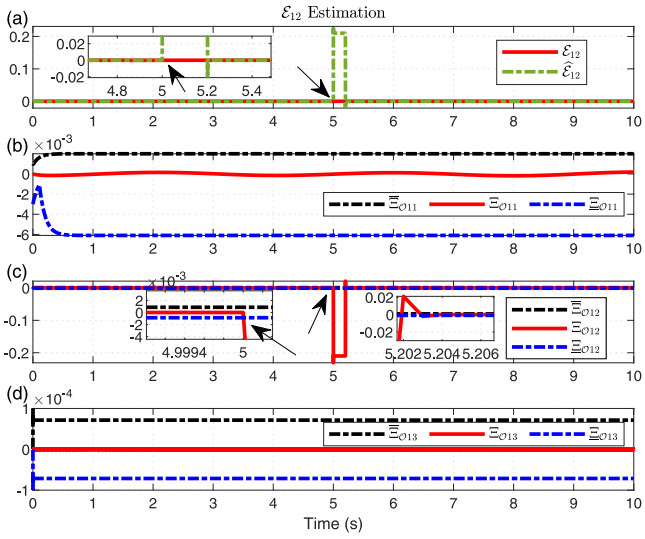

Fig. 8. Sensor fault detection and isolation for S2.

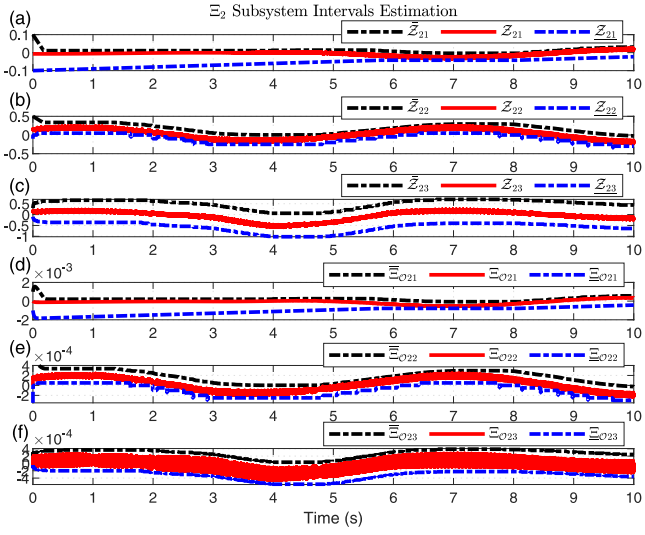

Fig. 9. Ξ_2 subsystem intervals estimation for S2.

4.2. S2

The proposed detection and isolation framework can effectively detect the sensor fault occurrence time moment and isolate the faulty sensor. Compared to S1, the initial values of the adaptive estimation interval bounds and the Luenberger and interval observer gains remain unchanged in S2. In this scenario, a fault occurs in the position sensor corresponding to $\mathcal{E}_{12}$. As in (53), the sensor fails at the time interval $[5, 5.2]$, namely, $\mathcal{S}_{12} = 0.21$, for $t \in [5, 5.2]$, else $\mathcal{S}_{12} = 0$.

As shown in Fig. 8(a) and (c), with the designed interval observer, it is easy to detect when a sensor failure occurs and to isolate the faulty sensor. Some simulation results similar to S1 are ignored in the subsection due to space limitations. It can be observed from Fig. 8(c) that the sensor fault causes $\Xi_{\mathcal{O}12}$ to be outside the estimated interval $[\underline{\Xi}_{\mathcal{O}12}, \overline{\Xi}_{\mathcal{O}12}]$. Specifically, the moment when the interval boundary is exceeded can be seen as the sensor fault occurs time. In addition, by further combining Fig. 8(b) and (d), the faulty sensor can be isolated. That is, it is easy to obtain that the position sensor corresponding to $\mathcal{S}_{12}$ is faulty.

Moreover, the interval estimation results for the b subsystem are depicted in Fig. 9(a)–(f), where the corresponding interval bounds

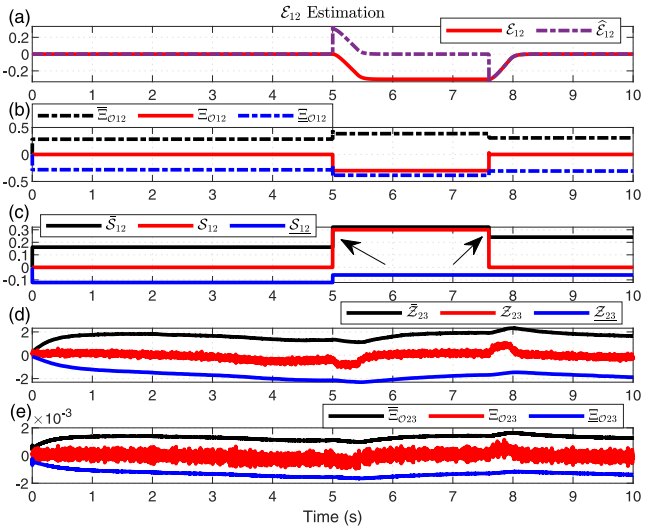

Fig. 10. Sensor fault estimation for S3.

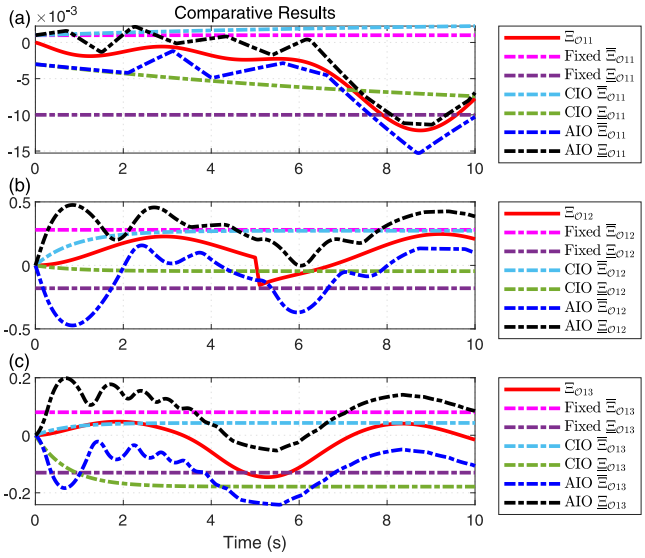

Fig. 11. Comparison results with existing methods.

still can be adaptively estimated effectively for sensors without faults. Accordingly, it concludes that effective detection and isolation of sensor faults can be achieved with the designed interval observer structure.

4.3. S3

By modifying the interval observer as Theorem 3, the sensor fault interval bounds can be estimated by (57)–((64)). In contrast to S1 and S2, the position sensor fault for S3 is set to $\mathcal{S}_{12} = 0.3$, for $t \in [5, 7.6]$, else $\mathcal{S}_{12} = 0$. The remaining observer parameters and initial values are the same as S2. The fault estimation parameters are chosen as $\overline{\mu_{11}} = 10^{-3}$, $\underline{\mu_{11}} = 10^{-3}$, $\ell_{11} = 1$, $\rho_{11} = 2$, $\overline{\mu_{12}} = 80$, $\underline{\mu_{12}} = 60$, $\ell_{12} = 0.02$, $\rho_{12} = 0.5$, $\overline{\mu_{13}} = 10^{-3}$, $\underline{\mu_{13}} = 10^{-3}$, $\ell_{13} = 0.002$, $\rho_{13} = 0.02$, $\overline{\mu_{21}} = 10^{-4}$, $\underline{\mu_{21}} = 10^{-4}$, $\ell_{21} = 0.001$, $\rho_{21} = 0.02$, $\overline{\mu_{22}} = 8$, $\underline{\mu_{22}} = 6$, $\ell_{22} = 0.18$, $\rho_{22} = 0.2$, $\overline{\mu_{23}} = 10^{-4}$, $\underline{\mu_{23}} = 10^{-4}$, $\ell_{23} = 0.001$, and $\rho_{23} = 0.002$. The corresponding initial values are $\overline{S_1}(0) = [10^{-3}, 10^{-3}, 10^{-5}]^T$, $\underline{S_1}(0) = [-10^{-3}, -10^{-3}, -10^{-5}]^T$, $\overline{S_2}(0) = [10^{-4}, 5 * 10^{-4}, 3 * 10^{-4}]^T$ and $\underline{S_2}(0) = [-10^{-4}, -10^{-4}, -10^{-4}]^T$.

As illustrated in Fig. 10(a), the sensor fault causes the sensor estimation $\hat{\mathcal{E}}_{12}$ deviates from the corresponding state $\mathcal{E}_{12}$. Unlike S2, by modifying the interval observer, the corresponding interval bounds estimations can be adaptively updated such that $\underline{\mathcal{S}_{12}} < \mathcal{S}_{12} < \overline{\mathcal{S}_{12}}$ holds, as in Fig. 10(b). Meanwhile, as in Fig. 10(c), the interval bounds for the sensor fault S12 can be estimated adaptively. Fig. 10(d) and (e) are provided as representative results to illustrate that the corresponding intervals for the fault-free sensors can also be adaptively estimated, and the rest of the similar results are ignored for simplicity. The simulation results in Fig. 10(a)–(e) illustrate that the modified interval observer can achieve an effective sensor fault estimation.

4.4. S4

To further analyze the advantages of the designed method, comparative results with existing fault diagnosis methods are provided. The fault (53) occurs in the position sensor corresponding to $\mathcal{E}_{12}$ with $\mathcal{S}_{12} = 0.2$, for $5 \leq t \leq 5.1$, else $\mathcal{S}_{12} = 0$. The following methods are implemented: (1) Fixed: Luenberger observer with a fixed threshold (Shen et al., 2018). (2) CIO: Fault diagnosis using a conventional interval observer (Zhang & Yang, 2017). (3) AIO: The proposed interval fault observer with adaptive estimation. The parameters are chosen as: C_1 :=diag(1, 11, 14), C_2 :=diag(54, 1, 18), $\overline{\alpha_{11}} = 0.05$, $\underline{\alpha_{11}} = 0.07$, $\gamma_{11} = 6 * 10^{-4}$, $\beta_{11} = 3 * 10^{-3}$, $\overline{\alpha_{12}} = 1$, $\underline{\alpha_{12}} = 1$, $\gamma_{12} = 0.1$, $\beta_{12} = 0.18$, $\overline{\alpha_{13}} = 1$, $\underline{\alpha_{13}} = 1$, $\gamma_{13} = 0.09$, $\beta_{13} = 0.1$, $\overline{\alpha_{21}} = 0.5$, $\underline{\alpha_{21}} = 0.01$, $\beta_{21} = 5 * 10^{-3}$, $\gamma_{21} = 2 * 10^{-4}$, $\overline{\alpha_{22}} = 1$, $\underline{\alpha_{22}} = 50$, $\beta_{22} = 2 * 10^{-3}$, $\gamma_{22} = 5 * 10^{-4}$, $\overline{\alpha_{23}} = 20$, $\underline{\alpha_{23}} = 10$, $\beta_{23} = 5 * 10^{-3}$, and $\gamma_{23} = 1 * 10^{-4}$.

The detailed comparative results are illustrated in Fig. 11. For the traditional fixed-threshold fault diagnosis method, as shown in Fig. 11(a) and (c), there are false alarms at $t \in (8, 10)s$ and $t = 5$ s. Because the threshold is exceeded, the fault occurrence is identified mistakenly for the healthy position sensor and angle sensor. And the occurred sensor fault is not detected as in Fig. 11(b), due to a large threshold. For the classical interval observer method, false alarms exist at $t \in (7, 10)s$ and $t = 2$ s as in Fig. 11(a) and (c). Meanwhile, CIO can also detect the sensor fault effectively as in Fig. 11(b), nevertheless, the sensitivity is reduced compared to the AIO. Using the proposed AIO framework, it can be observed from Fig. 11(b) that the occurred sensor fault is detected effectively. Moreover, for healthy sensors, there are no false alarms, as shown in Fig. 11(a) and (c). Clear adaptive updates can be seen in Fig. 11, which is the reason for the enhanced performance.

The classical fixed threshold method and the interval observer method rely on prior information to select an appropriate threshold. However, for a practical system, the health sensor may be misjudged as faulty by selecting a small threshold. When choosing a large threshold, the occurred sensor fault may be undetected. In contrast, with the designed AIO framework, the thresholds can be adaptively updated to improve fault sensitivity while effectively avoiding false alarms and missed alarms, as shown in Fig. 11. Moreover, the boundary information of the disturbances and uncertainties is unnecessary, which reduces the reliance on prior knowledge and makes it more applicable.

5. Conclusion

In this paper, a sensor fault detection, isolation, and estimation framework is designed for vehicle-integrated motion systems. It can be observed from simulation results that effective estimations of the state and the output interval bounds can be obtained when no sensor faults occur. The corresponding output caused by a sensor fault can exceed the estimated intervals. Thus, we can effectively detect the sensor fault occurrence moment and isolate the faulty sensor. When the proposed framework is reconstructed, the sensor fault can be estimated. Note that the proposed method is not only applicable to intelligent vehicle-integrated motion systems but can also be applied to quadrotor (Wang, Su, Han, & Chen, 2019), suspension (Huang, Wang, & Pan, 2023), linear motor (Liu & Sun, 2023), switched systems (Yan, Xia, Feng, & Zhang, 2023), robotic manipulators (Roveda, Forgione, & Piga, 2020; Yuan

& Sun, 2023), surface vehicles (*Guidance and control methodologies for marine vehicles: A survey*; Wang & Karimi, 2019; Wang, Karimi, Li, & Su, 2019; Wang & Su, 2019), etc. Future work focuses on the design of a fault-tolerant control (Wang, Pan, & Sun, 2022) scheme and taking actuator fault (Qiu, Wei, Karimi, & Gao, 2017) into account.

Declaration of competing interest

The authors declare that they have no known competing financial interests or personal relationships that could have appeared to influence the work reported in this paper.

Acknowledgments

This work was supported in part by the National Natural Science Foundation of China under Grant U1964201, Grant 62173108, and Grant 62022031; in part by the Post-Doctoral Science Foundation of Heilongjiang Province under Grant LBH-TZ2111; in part by the Major Scientific and Technological Special Project of Heilongjiang Province under Grant 2021ZX05A01; and in part by the Fundamental Research Funds for the Central Universities under Grant HIT.OCEF.2022012.

References

Blesa, J., Rotondo, D., Puig, V., & Nejjari, F. (2014). Fdi and ftc of wind turbines using the interval observer approach and virtual actuators/sensors. *Control Engineering Practice*, *24*, 138–155.

Borguet, S., & Léonard, O. (2009). Coupling principal component analysis and kalman filtering algorithms for on-line aircraft engine diagnostics. *Control Engineering Practice*, *17*(4), 494–502.

Chebotarev, S., Efimov, D., Raïssi, T., & Zolghadri, A. (2015). Interval observers for continuous-time lpv systems with l1/l2 performance. *Automatica*, *58*, 82–89.

Efimov, D., Raissi, T., & Zolghadri, A. (2013). Control of nonlinear and lpv systems: Interval observer-based framework. *IEEE Transactions on Automatic Control*, *58*(3), 773–778. http://dx.doi.org/10.1109/TAC.2013.2241476.

Feng, S., Sun, H., Yan, X., Zhu, H., Zou, Z., Shen, S., et al. (2023). Dense reinforcement learning for safety validation of autonomous vehicles. *Nature*, *615*(7953), 620–627.

Guidance and control methodologies for marine vehicles: A survey (2021). Control Engineering Practice, 111, Article 104785. http://dx.doi.org/10.1016/j.conengprac.2021.104785.

Havyarimana, V., Xiao, Z., Semong, T., Bai, J., Chen, H., & Jiao, L. (2023). Achieving reliable intervehicle positioning based on redheffer weighted least squares model under multi-gnss outages. *IEEE Transactions on Cybernetics*, *53*(2), 1039–1050. http://dx.doi.org/10.1109/TCYB.2021.3100080.

He, X., Wang, Z., & Zhou, D. (2009). Robust fault detection for networked systems with communication delay and data missing. *Automatica*, *45*(11), 2634–2639.

Holzmann, H., Halfmann, C., Germann, S., Würtenberger, M., & Isermann, R. (1997). Longitudinal and lateral control and supervision of autonomous intelligent vehicles. *Control Engineering Practice*, *5*(11), 1599–1605.

Huang, T., Pan, H., Sun, W., & Gao, H. (2022). Sine resistance network-based motion planning approach for autonomous electric vehicles in dynamic environments. *IEEE Transactions on Transportation Electrification*, *8*(2), 2862–2873.

Huang, T., Wang, J., & Pan, H. (2023). Adaptive bioinspired preview suspension control with constrained velocity planning for autonomous vehicles. *IEEE Transactions on Intelligent Vehicles*, 1–11. http://dx.doi.org/10.1109/TIV.2023.3273620.

Huang, T., Wang, J., Pan, H., & Sun, W. (2022). Finite-time fault-tolerant integrated motion control for autonomous vehicles with prescribed performance. *IEEE Transactions on Transportation Electrification*, 1. http://dx.doi.org/10.1109/TTE.2022.3232521.

Ji, H., He, X., Shang, J., & Zhou, D. (2017). Incipient fault detection with smoothing techniques in statistical process monitoring. *Control Engineering Practice*, *62*, 11–21.

Karimi, H. R., Chadli, M., Shi, P., & Zhang, L. (2014). Fault detection, isolation, andtolerant control of vehicles using soft computing methods. *IET Control Theory & Applications*, *8*(9), 655–657. http://dx.doi.org/10.1049/iet-cta.2014.0577.

Karimi, H. R., Duffie, N. A., & Dashkovskiy, S. (2010). Local capacity h_∞ control for production networks of autonomous work systems with time-varying delays. *IEEE Transactions on Automation Science and Engineering*, *7*(4), 849–857. http://dx.doi.org/10.1109/TASE.2010.2046735.

Karimi, H. R., & Gao, H. (2008). Mixed h_2/h_∞ output-feedback control of second-order neutral systems with time-varying state and input delays. *ISA Transactions*, *47*(3), 311–324.

Karimi, H. R., Zapateiro, M., & Luo, N. (2010). A linear matrix inequality approach to robust fault detection filter design of linear systems with mixed time-varying delays and nonlinear perturbations. *Journal of the Franklin Institute*, *347*(6), 957–973.

Kommuri, S. K., Defoort, M., Karimi, H. R., & Veluvolu, K. C. (2016). A robust observer-based sensor fault-tolerant control for pmsm in electric vehicles. *IEEE Transactions on Industrial Electronics*, *63*(12), 7671–7681.

Li, Y., Karimi, H. R., Zhang, Q., Zhao, D., & Li, Y. (2017). Fault detection for linear discrete time-varying systems subject to random sensor delay: A riccati equation approach. *IEEE Transactions on Circuits and Systems. I. Regular Papers*, *65*(5), 1707–1716.

Liu, Y., & Sun, W. (2023). High-performance position control for repetitive tasks of motor-driven servo systems based on periodic disturbance observer. *IEEE/ASME Transactions on Mechatronics*, 1–10. http://dx.doi.org/10.1109/TMECH.2023.3251998.

Oh, K., Park, S., Lee, J., & Yi, K. (2018). Functional perspective-based probabilistic fault detection and diagnostic algorithm for autonomous vehicle using longitudinal kinematic model. *Microsystem Technologies*, *24*(11), 4527–4537.

Pan, H., Chang, X., & Sun, W. (2023). Multitask knowledge distillation guides end-to-end lane detection. *IEEE Transactions on Industrial Informatics*, 1–10. http://dx.doi.org/10.1109/TII.2023.3233975.

Pan, H., Hong, Y., Sun, W., & Jia, Y. (2023). Deep dual-resolution networks for real-time and accurate semantic segmentation of traffic scenes. *IEEE Transactions on Intelligent Transportation Systems*, *24*(3), 3448–3460. http://dx.doi.org/10.1109/TITS.2022.3228042.

Pan, H., Zhang, C., & Sun, W. (2022). Fault-tolerant multiplayer tracking control for autonomous vehicle via model-free adaptive dynamic programming. *IEEE Transactions on Reliability*, 1–12. http://dx.doi.org/10.1109/TR.2022.3208467.

Pan, H., Zhang, D., Sun, W., & Yu, X. (2022). Event-triggered adaptive asymptotic tracking control of uncertain mimo nonlinear systems with actuator faults. *IEEE Transactions on Cybernetics*, *52*(9), 8655–8667. http://dx.doi.org/10.1109/TCYB.2021.3061888.

Pertew, A. M., Marquez, H. J., & Zhao, Q. (2007). Lmi-based sensor fault diagnosis for nonlinear lipschitz systems. *Automatica*, *43*(8), 1464–1469.

Puig, V., Stancu, A., Escobet, T., Nejjari, F., Quevedo, J., & Patton, R. J. (2006). Passive robust fault detection using interval observers: Application to the damadics benchmark problem. *Control Engineering Practice*, *14*(6), 621–633.

Qiu, J., Wei, Y., Karimi, H. R., & Gao, H. (2017). Reliable control of discrete-time piecewise-affine time-delay systems via output feedback. *IEEE Transactions on Reliability*, *67*(1), 79–91.

Raïssi, T., Videau, G., & Zolghadri, A. (2010). Interval observer design for consistency checks of nonlinear continuous-time systems. *Automatica*, *46*(3), 518–527.

Roveda, L., Forgione, M., & Piga, D. (2020). Robot control parameters auto-tuning in trajectory tracking applications. *Control Engineering Practice*, *101*, Article 104488.

Samy, I., Postlethwaite, I., & Gu, D.-W. (2011). Survey and application of sensor fault detection and isolation schemes. *Control Engineering Practice*, *19*(7), 658–674.

Shen, Q., Yue, C., Goh, C. H., & Wang, D. (2018). Active fault-tolerant control system design for spacecraft attitude maneuvers with actuator saturation and faults. *IEEE Transactions on Industrial Electronics*, *66*(5), 3763–3772.

Spielberg, N. A., Brown, M., Kapania, N. R., Kegelman, J. C., & Gerdes, J. C. (2019). Neural network vehicle models for high-performance automated driving. *Science Robotics*, *4*(28), Article eaaw1975.

Sun, W., Zhang, J., & Liu, Z. (2018). Two-time-scale redesign for antilock braking systems of ground vehicles. *IEEE Transactions on Industrial Electronics*, *66*(6), 4577–4586.

Wang, X. (2020). Active fault tolerant control for unmanned underwater vehicle with sensor faults. *IEEE Transactions on Instrumentation and Measurement*, *69*(12), 9485–9495.

Wang, N., & Deng, Z. (2019). Finite-time fault estimator based fault-tolerance control for a surface vehicle with input saturations. *IEEE Transactions on Industrial Informatics*, *16*(2), 1172–1181.

Wang, X., Fei, Z., Yan, H., & Xu, Y. (2020). Dynamic event-triggered fault detection via zonotopic residual evaluation and its application to vehicle lateral dynamics. *IEEE Transactions on Industrial Informatics*, *16*(11), 6952–6961.

Wang, N., Gao, Y., Zhao, H., & Ahn, C. K. (2020). Reinforcement learning-based optimal tracking control of an unknown unmanned surface vehicle. *IEEE Transactions on Neural Networks and Learning Systems*, *32*(7), 3034–3045.

Wang, N., & Karimi, H. R. (2019). Successive waypoints tracking of an underactuated surface vehicle. *IEEE Transactions on Industrial Informatics*, *16*(2), 898–908.

Wang, N., Karimi, H. R., Li, H., & Su, S.-F. (2019). Accurate trajectory tracking of disturbed surface vehicles: A finite-time control approach. *IEEE/ASME Transactions on Mechatronics*, *24*(3), 1064–1074.

Wang, J., Ma, J., Pan, H., & Sun, W. (2023). Event-triggered adaptive saturated fault-tolerant control for unknown nonlinear systems with full state constraints. *IEEE Transactions on Automation Science and Engineering*, 1–13. http://dx.doi.org/10.1109/TASE.2023.3237334.

Wang, J., Pan, H., & Sun, W. (2022). Event-triggered adaptive fault-tolerant control for unknown nonlinear systems with applications to linear motor. *IEEE/ASME Transactions on Mechatronics*, *27*(2), 940–949. http://dx.doi.org/10.1109/TMECH.2021.3075478.

Wang, J., Pan, H., & Zhang, D. (2023). Event-triggered adaptive finite-time control for mimo nonlinear systems with actuator faults. *IEEE Transactions on Industrial Electronics*, *70*(7), 7343–7352. http://dx.doi.org/10.1109/TIE.2022.3201291.

Wang, N., & Su, S.-F. (2019). Finite-time unknown observer-based interactive trajectory tracking control of asymmetric underactuated surface vehicles. *IEEE Transactions on Control Systems Technology*, *29*(2), 794–803.

Wang, N., Su, S.-F., Han, M., & Chen, W.-H. (2019). Backpropagating constraints-based trajectory tracking control of a quadrotor with constrained actuator dynamics and complex unknowns. *IEEE Transactions on Systems, Man, and Cybernetics: Systems*, *49*(7), 1322–1337. http://dx.doi.org/10.1109/TSMC.2018.2834515.

Wang, S., & Xiao, F. (2004). Ahu sensor fault diagnosis using principal component analysis method. *Energy and Buildings*, *36*(2), 147–160.

Wang, N., Zhang, Y., Ahn, C. K., & Xu, Q. (2021). Autonomous pilot of unmanned surface vehicles: Bridging path planning and tracking. *IEEE Transactions on Vehicular Technology*, *71*(3), 2358–2374.

Yan, S., Sun, W., He, F., & Yao, J. (2018). Adaptive fault detection and isolation for active suspension systems with model uncertainties. *IEEE Transactions on Reliability*, *68*(3), 927–937.

Yan, J., Xia, Y., Feng, X., & Zhang, Y. (2023). Deception attack detection based on bandwidth allocation for switched systems with quantization. *Automatica*, *154*, Article 111094. http://dx.doi.org/10.1016/j.automatica.2023.111094.

Yuan, Y., & Sun, W. (2023). An integrated kinematic calibration and dynamic identification method with only static measurements for serial robot. *IEEE/ASME Transactions on Mechatronics*, 1–12. http://dx.doi.org/10.1109/TMECH.2023.3241302.

Zhang, J., Sun, W., & Du, H. (2019). Integrated motion control scheme for four-wheel-independent vehicles considering critical conditions. *IEEE Transactions on Vehicular Technology*, *68*(8), 7488–7497.

Zhang, Z.-H., & Yang, G.-H. (2017). Interval observer-based fault isolation for discrete-time fuzzy interconnected systems with unknown interconnections. *IEEE Transactions on Cybernetics*, *47*(9), 2413–2424.